Evaluation of baseflow estimation methods with real and synthetic streamflow data from a watershed

by

Siyu Cheng

A thesis

presented to the University of Waterloo

in fulfillment of the

thesis requirement for the degree of

Master of Science

in

Earth Science

Waterloo, Ontario, Canada, 2022

Author's Declaration

I hereby declare that I am the sole author of this thesis. This is a true copy of the thesis, including any required final revisions, as accepted by my examiners.

I understand that my thesis may be made electronically available to the public.

Abstract

Baseflow with origins from groundwater is a critical component of streamflow sustaining it throughout the year especially during dry periods. To better understand the role of baseflow in streamflow, accurate estimates are needed. This study calculates baseflow through existing graphical and digital filter methods, using actual streamflow data from a gauging station at the Alder Creek Watershed (ACW) and synthetic streamflow data at ten study points within the same watershed simulated with HydroGeoSphere (HGS) (Aquanty Inc., 2018). There are four widely used graphical (Sloto and Crouse, 1996; Aksoy et al., 2008) and six digital filter (Lyne and Hollick, 1979; Chapman and Maxwell, 1996; Furey and Gupta, 2001; Eckhardt, 2005; Tularam and Ilahee, 2008; Aksoy et al., 2009) approaches for baseflow estimation being used and compared. To determine the most optimal estimation approach, baseflow estimates from real data are assessed based on the concept of hydrologic plausibility (Nathan and McMahon, 1990), while baseflow estimates obtained from the HGS streamflow record with graphical and digital filter methods are compared to those computed directly by HGS. Overall, results from this study indicate that baseflow hydrographs reveal a seasonal pattern. During wintertime, streamflow is composed almost entirely of baseflow, whereas during summertime, baseflow only consists approximately 20% to 60% of streamflow. After comparing the baseflow estimates with those computed by HGS, the most optimal approaches at ten points are assessed. Results show that the best approach for six points is the FUKIH (Aksoy et al., 2009) approach; for three points is the Chapman and Maxwell (1996) approach; and for one point is the Eckhardt (2005) approach. In conclusion, it is inferred that the most optimal approach within the ACW varies spatially.

Acknowledgements

I would like to express my gratitude to my supervisor Professor Walter A. Illman for joining his research group and giving me an opportunity to learn from him. He has provided me extensive patient guidance and encouragement, and I benefit a lot from his constructive suggestions during the development of research work. His willingness to give his time has been very much appreciated.

I would like to thank my committee members Dr. David Rudolph and Dr. Andrea Brookfield, for taking their time to attend the committee meetings and providing me with valuable comments on how to improve the project.

I would like to thank my colleagues and friends for their support, who include Xin Tong, Vanessa Lu, Jasmine Qu, and Zhejun He. Special thanks go to Xin Tong, for looking over my paper carefully and helping me with numerous questions during the two years, and also thanks for providing the essential data needed in my project.

Finally, I wish to thank my parents for their support throughout my study.

Table of Contents

List of Figures

List of Tables

Chapter 1

Introduction

Baseflow is an essential component of streamflow, which originates primarily from groundwater discharging into streams (e.g., Hall, 1968; Freeze, 1972; Eckhardt, 2005; Brodie et al., 2007). As an important component of streamflow, baseflow plays an essential role in sustaining riparian and aquatic ecosystems as well as having impacts on stream water chemistry. In many streams, streamflow is primarily composed of baseflow during dry periods, and during wet seasons, the ratio of baseflow to streamflow could decrease significantly depending on site conditions. For example, in a dry climate, baseflow has been estimated to be approximately 80 percent within the Upper Colorado River Basin (Miller et al., 2016). In the baseflow and water use assessment report by Toronto and Region Conservation (2008), baseflow has been estimated to be approximately 40 percent from the Don River Watershed in a humid climate during summertime.

In contrast to baseflow, surface runoff is the quick response to rainfall events containing precipitation falling directly onto streams, overland flow, and interflow or throughflow. It constitutes a larger portion of the streamflow during wet seasons. Predicting the contribution of baseflow relative to streamflow is essential for watershed management that could help determine the potential discharge that may occur during a rainy season or a flooding period (Indarto et al., 2016).

Research on baseflow characteristics is vital for comprehending runoff generation processes and understanding interactions among streamflow, groundwater, and other components of the water cycle. Moreover, investigations on spatial and temporal variability

of baseflow could lead to a better quantification of the significance of groundwater in streamflow processes. Furthermore, a detailed understanding of these water cycle components and how these components vary with space and time could lead to better solutions to water quantity and quality issues within a watershed. Due to this importance, studies on estimating baseflow through various approaches have been widely conducted (e.g., Winter et al., 1998; Cey et al., 1998; Kalbus et al., 2006; Rosenberry and LaBaugh, 2008). However, it is difficult to obtain accurate baseflow hydrographs directly and continuously in the field. Therefore, many different approaches have been developed to estimate baseflow based on different kinds of data that are available within a watershed.

Baseflow estimation methods can be roughly divided into three groups: direct measurements, tracer-based estimation, and non-tracer-based estimation methods. Direct measurements rely on different instruments to measure baseflow values at discrete points. Tracer-based estimation methods mainly rely on chemical tracers to explore the generation processes of each water cycle component (Yu and Schwartz, 1999). Non-tracer-based estimation methods could be subdivided into several groups, including graphical and digital filter methods. In graphical methods, different criteria are used to separate streamflow into baseflow and surface runoff through the analysis of a streamflow hydrograph. In digital filter methods, numerical approaches are utilized to filter streamflow into different portions of the hydrograph.

In previous research on baseflow estimation, various approaches have been utilized and then compared to evaluate the results (e.g., Nathan and McMahon, 1990; Cey et al., 1998; Chapman, 1999; Arnold et al., 2000; Smakhtin, 2001; Conant, 2004; Schwartz, 2007; Gonzales et al., 2009; Indarto et al., 2016; Lott and Stewart, 2016; Xie et al., 2020; Kissel

and Schmalz, 2020). For example, Cey et al. (1998) compared four field approaches to measure baseflow values at a small watershed in southern Ontario, Canada. Approaches compared include the use of the velocity-area technique, mini piezometers measurements, seepage meter measurements, and analyses of electrical conductivity as well as isotope data. Among the first three techniques, the velocity-area technique resulted in the best baseflow estimates. From the analyses of isotope and electrical conductivity data, it was shown that during storm events, pre-event water contributed approximately 64% to 80% of total discharge, and antecedent moisture conditions of the catchment were found to largely affect the percentage of event- and pre-event water in streamflow.

Conant (2004) developed a method that related fluxes from minipiezometers to streambed temperatures. Then, a generalized conceptual model of groundwater discharge was developed based on groundwater flux data determined through geochemical data from a stream in Angus, Ontario, Canada. This conceptual model could be used to evaluate groundwater discharge and subdivided discharge behaviors into five categories, which were short-circuit discharge, high discharge, low to moderate discharge, no discharge, and recharge.

Gonzales et al. (2009) compared various baseflow estimation methods, including both tracer- and non-tracer-based methods in a lowland area of the Netherlands. The hydrological tracer approach revealed that groundwater responded quickly to rainfall events in this area, and surface water contributed most of the measured discharge during flood events. Moreover, the estimated results were compared with baseflow values determined through the tracer-based method. In their study, Gonzales et al. (2009)

concluded that the rating curve method and the recursive filtering method proposed by Eckhardt (2005) resulted in reliable baseflow values.

Indarto et al. (2016) reviewed earlier work on baseflow estimation and used seven recursive digital and two graphical methods in East Java, Indonesia to determine the optimal parameters values, baseflow index, and to find the appropriate method for the investigated watershed. Results revealed that the exponentially weighted moving average (EWMA) approach (Tularam and Ilahee, 2008), the Lyne and Hollick approach (1979), and the local-minimum method (Sloto and Crouse, 1996) performed better in this area.

Lott and Stewart (2016) analyzed six baseflow estimation methods for 35 representative stream gages located across the United States including two graphical approaches—HYSEP fixed- and sliding-interval approaches (Sloto and Crouse, 1996), two baseflow index approaches (Wahl and Wahl, 1995), power function (Lott and Stewart, 2013), and WHAT technique (Lim et al., 2005), which is a software that incorporates the Lyne and Hollick (1979) as well as Eckhardt (2005) approaches. The results were compared with baseflow derived from the conductivity mass balance (CMB) method. The correlation coefficients of these analytical methods showed that HYSEP methods had the lowest correlation with the CMB method. Once these analytical methods were calibrated to CMB data, the correlation coefficients of these methods all increased significantly from 0.35 to 1.00, which suggests a better correspondence of estimated baseflow between analytical and CMB approaches.

Xie et al. (2020) estimated baseflow values with four graphical and five digital filter methods for 1,815 catchments in the United States. An evaluation criterion was established to determine the true baseflow, and this evaluation criterion was used together with some

performance metrics to analyze the accuracy of each estimation method. In this evaluation criterion, they selected streamflow values during low flow conditions and treated these streamflow values strictly as baseflow values. Low flow conditions were defined as the condition when quick flow, which includes interflow and overland flow, has ceased in a catchment. Through this evaluation criterion, Xie et al. (2020) concluded that the Eckhardt (2005) method had the best performance across the contiguous United States based on the evaluation results for 1,815 catchments.

In these previous studies, several baseflow estimation methods were utilized and evaluated. However, as mentioned previously, baseflow values are notoriously hard to quantify over long-time scales especially within a large study area. Actual baseflow values from a watershed are always absent to help determine the best estimation technique. Most studies have determined the optimal baseflow estimation technique simply based on the concept of hydrologic plausibility (Nathan and McMahon, 1990) such as the delayed response behavior of baseflow (Xie et al., 2020), considered to be highly subjective and may lead to biased results. Some studies have used the chemical tracer approach to estimate baseflow values, such as in the study conducted by Gonzales et al. (2009). However, the requirement of large quantities of chemical tracer data over an entire catchment can be costly, thus may not always be feasible.

Some researchers have used fully integrated three-dimensional surface water/groundwater physical models under different hydrological conditions to simulate baseflow values, and the synthetic baseflow were assumed to be the true baseflow to test various baseflow estimation techniques (e.g., Partington et al., 2012; Li et al., 2014; Su et al., 2016). In particular, Partington et al. (2012) used four approaches to estimate baseflow

values including the HYSEP approach (Sloto and Crouse, 1996), the PART program (Rutledge, 1998) that is constructed based on a graphical approach, the BFLOW program (Arnold and Allen, 1999) constructed based on the Lyne and Hollick (1979) approach, and the Eckhardt approach (2005). To test the performance of each approach, HydroGeoSphere (HGS) (Aquanty Inc. 2018) in conjunction with a hydraulic mixing-cell (HMC) approach were used to obtain the synthetic, true baseflow values for a simple, monotonically sloping V-shaped catchment. Partington et al. (2012) found that the performance of different baseflow estimation approaches varied under eight different scenarios with different hydrological conditions, and the estimated baseflow ranged from 28% above to 64% percent lower compared to synthetic baseflow. Overall, HYSEP sliding-interval approach showed the best results in most scenarios in this study.

Similar to the work of Partington et al. (2012), Li et al. (2014) used the synthetic results from HGS of a simple V-shaped catchment to test the accuracies of three recursive digital filters and obtained the optimal parameters for these filters. The recursive filters tested in this study were the Lyne and Hollick approach (1979), Chapman and Maxwell (1996), Boughton two-parameter filter (Boughton, 1993; Chapman, 1999), and Eckhardt (2005) approaches. Results showed that the baseflow estimates obtained through the Lyne and Hollick filter could better match the HGS synthetic baseflow under a larger range of catchment hydrological characteristics, and the optimal parameters varied based on hydrological conditions.

Su et al. (2016) investigated the utility of hydrological signatures to calibrate the Eckhardt filter method and tested seven possible hydrological signatures of baseflow, comparing against the synthetic baseflow values simulated with HGS by Li et al. (2014)

for a tilted V-shaped catchment. Results showed that the Eckhardt filter had better performance after a hydrological signature-based calibration.

In these previous studies (Partington et al., 2012; Li et al., 2014; and Su et al., 2016), HGS was used to simulate baseflow with the HMC approach to help evaluate the performances of baseflow estimation approaches. Although the use of synthetic baseflow from a model solved the problem of lacking true baseflow estimates from an actual site, synthetic baseflow used in these studies was not simulated for a real watershed. Instead, the analysis was conducted based on a monotonically sloping V-shaped catchment, that simplifies the intricate environmental conditions in actual watersheds subjected to seasonal hydrologic variations.

In this study, the primary purpose is to estimate baseflow values from streamflow data at the Alder Creek Watershed (ACW) in southern Ontario, Canada. Baseflow estimation is conducted through ten different approaches including four graphical and six digital filter approaches. Graphical methods include: the 1) United Kingdom Institute of Hydrology (UKIH) method (Aksoy et al., 2008); 2) three hydrograph-separation (HYSEP) methods, which are fixed-interval (HYSEP1), sliding-interval (HYSEP2), and local-minimum (HYSEP3) methods (Sloto and Crouse, 1996). Digital filter approaches include those developed by: 1) Lyne and Hollick (1979); 2) Filtered United Kingdom Institute of Hydrology (FUKIH) approach (Aksoy et al., 2009); 3) Chapman and Maxwell (1996); 4) Eckhardt (2005); 5) Furey and Gupta (2001); and the 6) EWMA approach (Tularam and Ilahee, 2008). Baseflow estimates obtained through the ten approaches using actual streamflow data from a real streamflow gauge are first compared and assessed utilizing the concept of hydrologic plausibility (Nathan and McMahon, 1990).

As true baseflow estimates from the ACW are not available to properly evaluate the performance of various baseflow separation techniques, synthetic streamflow and baseflow data obtained from HGS are utilized for a more rigorous comparison of various techniques. Unlike the simple V-shape catchment models used by Partington et al. (2012) and Li et al. (2014), actual hydrological and geological conditions of the ACW are simulated with HGS that rigorously considers the coupling of surface water, groundwater flow, and other hydrological conditions for the ACW (Tong et al. 2022). Although numerical models may not be able to provide actual baseflow values for a given site, the use of a fully 3D integrated hydrological model could still generate good independent conceptualization of watershed flow dynamics under different conditions until better baseflow estimation tools or observation techniques are developed (Partington et al., 2012). Through the HGS model used for this study, synthetic baseflow at ten different points in the ACW are obtained and assumed to be the true baseflow. These results are then compared against baseflow estimates obtained through the ten different baseflow estimation methods to determine the most optimal approach for the ACW.

Chapter 2

Site description and data used for analysis

2.1 Site description

The study area is the Alder Creek Watershed (ACW), which is situated at the southwestern portion of the Grand River Watershed located in southern Ontario, Canada (Figure 1), covering an area of approximately 79 km^2 (GRCA, 2009). In the central portion

of the Grand River Watershed, where the ACW is located, surficial material is predominantly comprised of glacial sediments.

Figure 2 shows that the ACW is covered by a large variety of surficial materials including clay, gravel, sand, and silt. More specifically, the middle and the southeastern portion of the ACW is predominately covered by poorly to well sorted fine sand and gravel to coarse sand; the southwestern part is mainly covered by poorly to well sorted fine gravel and sand to coarse gravel; and clay till is mostly distributed at the northern edge. These surficial sediments are mainly formed during the most recent episode of Pleistocene glaciation, which is the Wisconsinan glacial event, that commenced 25,000 years ago and approximately ended 10,000 years ago. The Wisconsinan glaciation is subdivided into different phases, thus the sediments deposited during different episodes are present within the ACW. Specifically, the bulk of glacial sediments found in this area contain pre-Michigan sub-episode tills, non-glacial sediments, Michigan sub-episode tills, as well as stratified sediments deposited by a regionally thick ice and oscillating lobate ice formed due to the advance and retreat of the Wisconsinan Ice Sheet (GRCA, 2018).

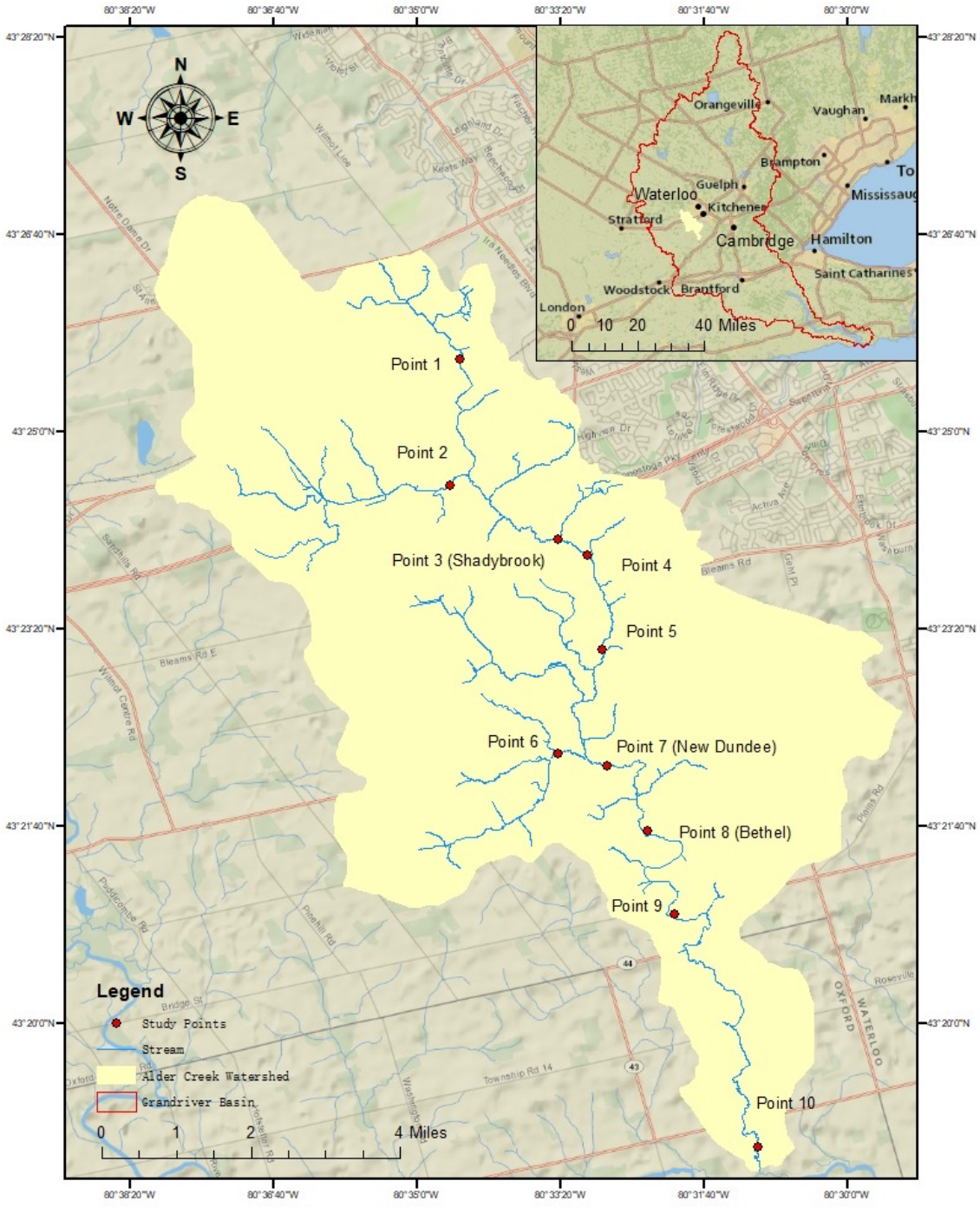

Figure 1. Location of the Alder Creek Watershed (ACW) and the distribution of ten study points. The small inset figure shows the location of the ACW in relation to the Grand River Watershed.

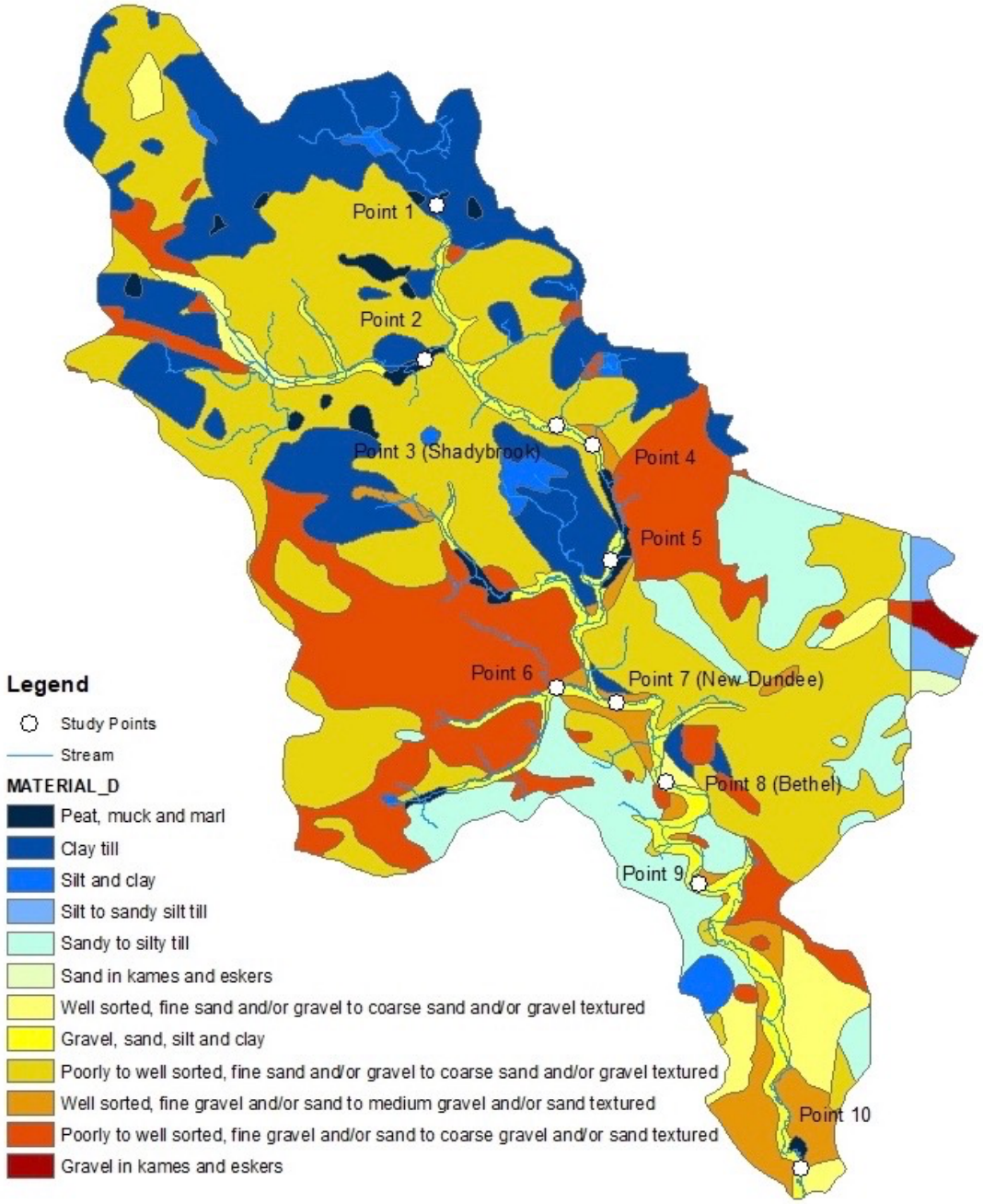

Figure 2. Map of surficial materials at the ACW showing the location of ten monitoring points in the HGS model. Data on surficial material are obtained from the Government of Ontario, Ministry of Northern Development, Mines, Natural Resources and Forestry (Government of Canada, 2019).

Beneath the surficial sediments, the bedrock beneath the watershed constitutes a portion of the Michigan and Appalachian Basins, which were deposited on the ocean floor by Devonian, Silurian, and Ordovician aged marine sediments that inundated this area

between 345 to 370 million years ago (GRCA, 2009). Moreover, the sedimentary bedrock around this area is mainly interbedded limestone, dolomite carbonate material, and the shale of the oldest Ordovician to the youngest Devonian (GRCA, 2009).

As for land use, a total of seven categories have been classified. Figure 3 shows that the ACW is predominately used for agriculture, with fully 70 percent of which is used as agricultural land. Other than agricultural land, land use within the watershed area consists also of urban built-up, forest, open water, grassland areas, golf course area, as well as aggregate extraction and roads.

In terms of site hydrology, the ACW has a humid continental climate with an annual precipitation ranging from 800 to 1,000 mm/year, and an average daily temperature ranging from -12.2 ℃ to 21.0 ℃ (Chow et al., 2016). During spring and fall, the weather is wet with an average daily temperature of ~5.0 ℃ and the precipitation is in the range of 100 mm/month, whereas the weather is dry during the summer with an average daily temperature of ~18.0 ℃ and the precipitation ranges from 30 to 40 mm/month. During winter, the average daily temperature is extremely low which is ~ -11.2 ℃, and the precipitation is mainly in the form of snowfall (Government of Canada, 2020). The annual snowfall in this watershed is ~150 - 200 cm, and the average annual evapotranspiration is estimated to be 500 - 600 mm/year (GRCA, 2009).

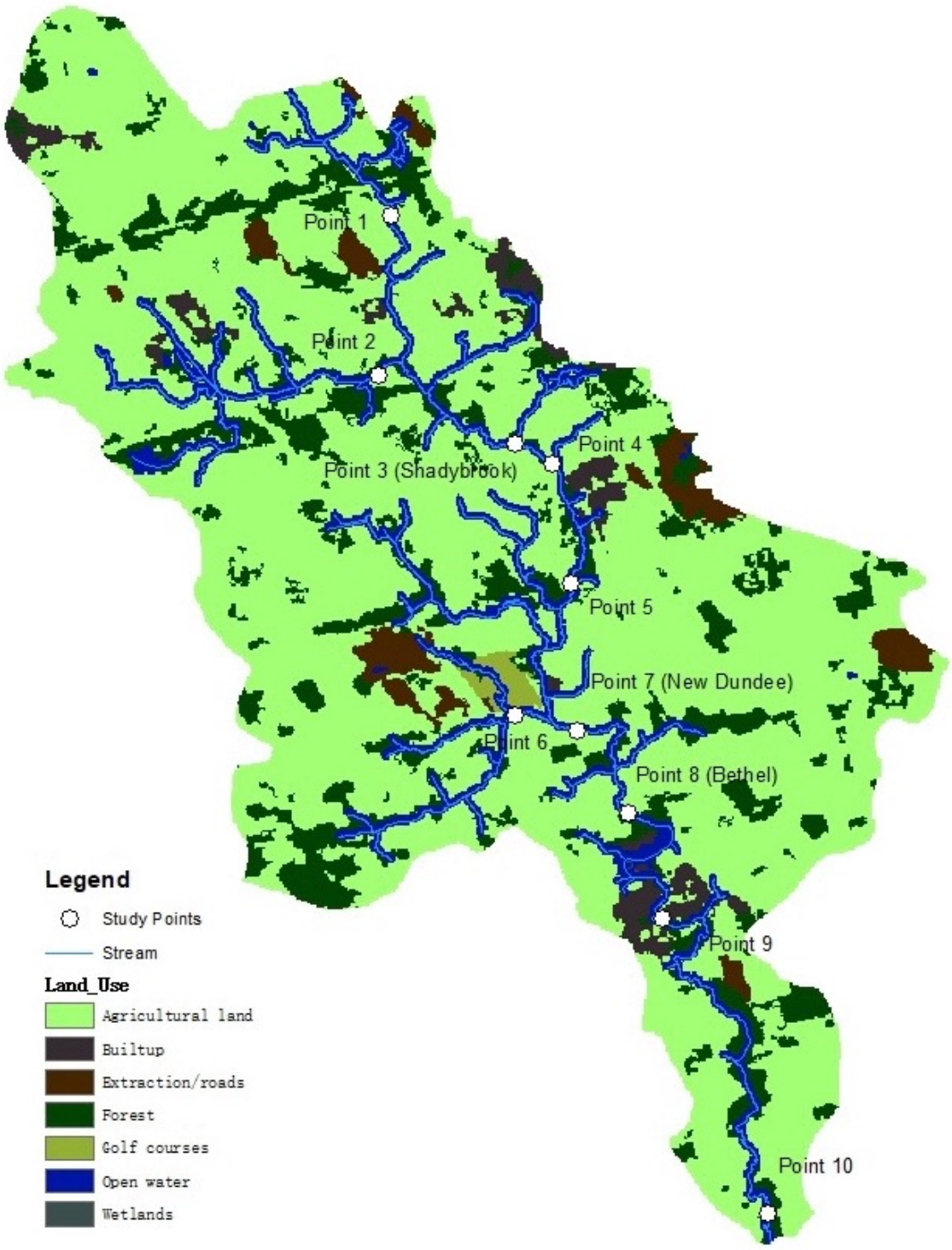

Figure 3. Land use map of the ACW showing the location of ten monitoring points in the HGS model. Land use data are obtained from the Grand River Conservation Authority (GRCA, 2019).

2.2 Research data

This study investigates the performances of non-tracer-based baseflow estimation approaches, which mainly rely on streamflow data to estimate baseflow values. In this study, the streamflow data used includes actual streamflow and synthetic streamflow data sets. Actual streamflow data is a three-year daily streamflow record from May 1st, 2013 to December 31st, 2016 at the New Dundee gauging station maintained by Environment and Natural Resources of Canada.

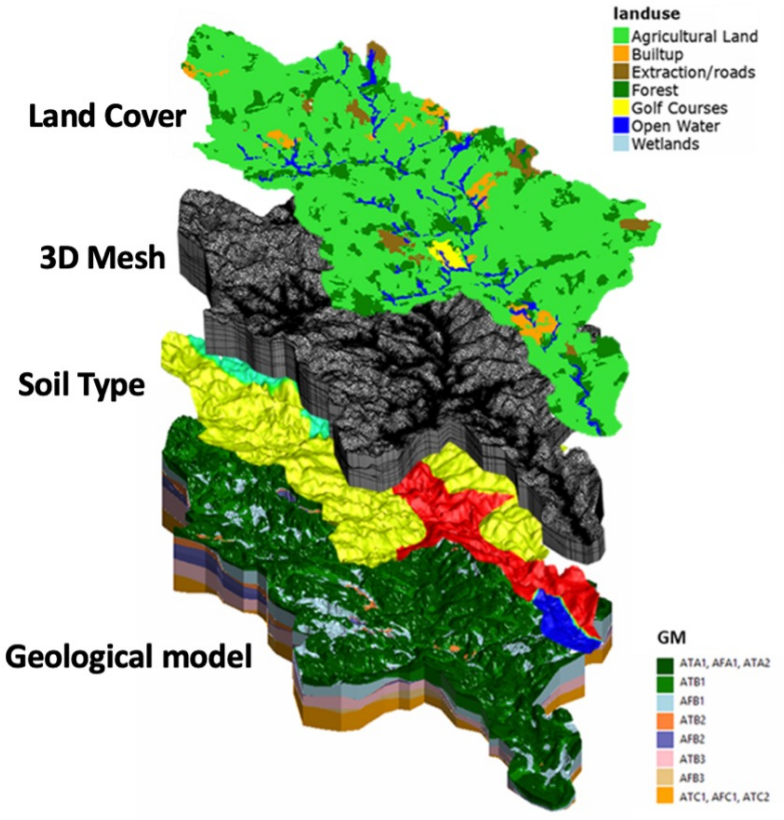

Figure 4. Components of the HydroGeoSphere (HGS) model constructed for the ACW by Tong et al. (2022) and utilized to generate synthetic streamflow and baseflow hydrographs. This HGS model is comprised of four components: land cover, 3D mesh, soil layer, and geological model. In the geological model, there are eight layers each with homogeneous hydraulic parameters.

As true baseflow estimates are not available at any location throughout the ACW, synthetic streamflow and baseflow hydrographs over a three-year period are also generated

with HydroGeoSphere (HGS) (Aquanty, 2018), a 3D fully integrated hydrological model that rigorously considers the coupling of surface water and groundwater flow processes (Tong et al., 2022).

The HGS model is composed of a surficial land use layer, 30 meter-resolution DEM data from Ontario Ministry of Natural Resources and Forestry, soil layer, and geological models through previously developed groundwater flow models (Figure 4) (Tong et al., 2022). In surficial land use layer, 25 meter-resolution land use data is utilized to describe plant functional types and surface roughness, and the data is obtained from the Grand River Conservation Authority (GRCA, 2009). Within the land use layer, there are seven land use types defined: forest, agricultural land, built-up, roads, golf courses, water, and wetland. Beneath the surficial layer, there is a 1-m deep soil layer defined with soil data from Soil Landscapes of Canada (SLC) compiled by Agricultural and Agri-Food Canada. In this soil layer, there are four soil types identified based on the soil texture.

The stratigraphic units below originate from the geological model of the FEFLOW model utilized for the Regional Municipality of Waterloo Tier Three Assessment (Matrix and SSPA, 2014a, b). Figure 4 shows that this geological model contains the layers of Aquifer A (AFA), Aquifer B (AFB), Aquifer C (AFC), Aquitard A (ATA), Aquifer B (ATB), Aquifer C (ATC), and these layers consist of different geological materials—ATA1: Whittlesey clay; AFA1: Whittlesey sand; ATA2: Wentworth Till; ATB1: Upper Maryhill Till, Port Stanley, Tavistock, Mornington and/or Stratford Tills; AFB1: Upper Waterloo Moraine Stratified Sediments and equivalents; ATB2: Middle Maryhill Till and equivalents; AFB2: Middle Waterloo Moraine Stratified Sediments and equivalents; ATB3: Lower Maryhill and stratified equivalents; AFB3: Lower Waterloo Moraine Stratified

Sediments or Catfish Creek Till Outwash; ATC1: Upper/Main Catfish Creek Till; AFC1: Middle Catfish Creek Stratified Deposits; and ATC2: Lower Catfish Creek Till (Matrix and SSPA, 2014a, b). When synthetic baseflow and streamflow are generated through the HGS model, winter processes are also considered. The snow, precipitation, and temperature data are utilized and applied to the model to conduct the transient simulations. The winter (November 1st to April 30th) simulation is considered after the completion of the simulation from spring to fall (May 1st to October 31st), and during the winter simulation, winter processes and winter parameters are added into the HGS model, including: 1) the freezing and thawing of porewater with lower hydraulic conductivity than summer that controls the flow of water (Schilling et al., 2019); and 2) the surface water flow with snowmelt and winter process (Tong et al., 2022).

Precipitation data from May 1st, 2013 to December 31st, 2016 utilized in the study are from the Roseville Environment Canada weather station, which is located just over 2 km outside the watershed. These precipitation events during this period are applied to the model. The exchange flux between the surface water and groundwater in the model is positive when the water flows from the soil surface down through the shallow subsurface and into the underlying aquifers as groundwater recharge, while the flow rate is negative when water moves out of the aquifers to the surface as groundwater discharge.

Ten monitoring points along the tributaries and the main stem of Alder Creek are selected where synthetic streamflow and baseflow hydrographs are recorded during the three-year simulation period. The ten monitoring points were selected by considering various factors such as the relative position within the watershed (i.e., tributary or main stem), surficial geology, exchange flux values, land use, and proximity to pumping wells.

The estimated baseflow from the HGS model at one point is simulated by summing the groundwater recharge and discharge values along the river upstream of the point during each timestep. Further details to the HGS model for the ACW and the computed synthetic baseflow are provided in Tong et al. (2022).

Chapter 3

Baseflow estimation methods

Baseflow estimation methods could be roughly divided into three groups: physically-based baseflow estimation methods, tracer-based methods, and non-tracer-based methods. In physically-based measurements, baseflow is directly measured through different instruments. In tracer-based estimation methods, chemical tracers are tracked to explore the generation processes of each water cycle component (Yu and Schwartz, 1999).

Non-tracer-based estimation methods could be subdivided into several groups, including graphical and digital filter methods. Graphical methods rely heavily on streamflow hydrographs to separate the surface runoff and baseflow. Digital filter methods are numerical approaches that are widely used for baseflow estimation. In digital filter methods, streamflow is defined to be composed of low-frequency and high-frequency components. Baseflow is assumed to be the low-frequency part of the streamflow that responds slowly to precipitation, and quick flow, including direct precipitation, interflow, and surface runoff, is the high-frequency part that responds quickly to precipitation.

3.1 Physically-based baseflow estimation methods

In physically-based baseflow estimation approaches, different instruments are used to measure the baseflow values directly in the field, such as seepage meter, mini-piezometer, heat pulse meter, and ultrasonic meter. These instruments are installed to measure the water fluxes across the groundwater – surface water interface. While direct measurements are very desirable, they typically only provide point estimates. In addition, direct measurements are always time-consuming and are not viable in making measurements at a large number of points within a watershed and over a long-time scale. Such point measurements are also logistically difficult to conduct in larger rivers, where access to measurement sites can be limited.

3.2 Tracer-based methods

In tracer-based methods, conservative tracers, including stable isotopes and other environmental tracers are utilized to separate streamflow into surface runoff and baseflow. When estimating baseflow using the chemical mass balance approach, it is assumed that streamflow components have differentiable isotopic or hydrochemical concentrations (Sklash and Farvolden, 1979). The following two equations are established based on mass balance considerations (Stewart et al., 2007):

$$c_{i,1}q_1 + c_{i,2}q_2 + \cdots + c_{i,j}q_j + \cdots c_{i,n}q_n = c_{i,T}q_T \quad (1)$$

$$q_1 + q_2 + \cdots + q_j + \cdots + q_n = q_T \quad (2)$$

where q_j (m^3/s) is the contribution of the flow component *j* to the total discharge, $c_{i,j}$ (ppm) is the concentration of chemical tracer *i* in the flow component *j*, q_T (m^3/s) is the total discharge, and $c_{i,T}$ (ppm) is the concentration of chemical solute *i* in the total discharge.

In Equations 1 and 2, (n−1) tracers are required to separate n different flow components in the total discharge. In most baseflow estimation cases, streamflow is simply

divided into baseflow and surface runoff, hence only one isotopic or hydrochemical component is required. There are several assumptions embedded in this approach. It is assumed that: 1) the isotopic or hydrochemical concentration is distinguishable for each component, 2) each component, such as precipitation, overland flow, and groundwater, is assumed to maintain a constant tracer concentration, and 3) the total amount of tracer is constant (Hooper and Shoemaker, 1986).

In previous studies, tracer-based estimation approaches have been widely used to determine baseflow values. However, tracer-based methods are always laborious and require time and effort. In addition, compared with non-tracer-based methods, tracer-based methods have high data and sampling requirements. These methods are also costly due to the expensive analysis of samples and could not be applied to past discharge time series due to a lack of required chemical data (Gonzales et al., 2009). Moreover, under field conditions, the assumptions for this approach may not be satisfied. These tracer-based methods may contain relatively large uncertainties from chemical reactions during the mixing of components, tracer measurements, and elevation effects on the isotopic composition of precipitation (Gonzales et al., 2009). Also, in tracer-based methods, only the advective movements of solute could be shown through chemical tracers, and the movements that are not advective might be ignored, and biased results might be caused. These uncertainties in chemical reactions could result in tracer concentration changes during water movement through the watershed, thus leading to less reliable baseflow estimation results. Therefore, alternative non-tracer-based methods to determine baseflow are needed and described next.

3.2 Non-tracer-based methods

3.2.1 Graphical methods

Graphical methods are commonly utilized to estimate baseflow through a streamflow hydrograph. In graphical methods, the relative minimum value of streamflow within a time interval is defined to be the baseflow value in that interval. How the relative minimum values and time interval are defined varies for different graphical methods. Then, the baseflow hydrograph is formed by connecting these relative minimum points. The following briefly summarizes each of these graphical approaches.

3.2.1.1 UKIH (2008) method

The UKIH method is a smoothed minima baseflow estimation method developed by the United Kingdom Institute of Hydrology (1980) and then adopted by Aksoy (2008). This approach could be applied to both ephemeral and perennial streams. In the UKIH approach, the time interval and the relative minimum values used for the target watershed are determined by the following functions:

$$N = 1.6A^{0.2} \tag{3}$$

where N is the block size in days and A is the watershed area in square miles.

The following steps are taken to find the relative minimum points:

a) Divide the daily streamflow into several non-overlapping intervals of N days.

b) Mark the minima of each interval, and define them as Q_1, Q_2, …, Q_t.

c) Divide the minima into groups (Q_1, Q_2, Q_3), (Q_2, Q_3, Q_4), (Q_{t-1}, Q_t, Q_{t+1}).

   For perennial streams, if $0.9Q_t < \min(Q_{t-1}, Q_{t+1})$; for ephemeral streams, if $0.9Q_t \leq \min(Q_{t-1}, Q_{t+1})$, then the central value is defined to be a relative minimum point.

d) Connect these relative minimum points by straight lines to form the baseflow hydrograph. If baseflow estimated by this line exceeds streamflow, baseflow is set to be equal to total flow.

For the ACW, A is equal to 79 km^2, hence, a four-day interval is considered in this study.

The principle and the procedure of the UKIH method are systematic. Consequently, this method can be used to build a user-friendly baseflow separating computer program (Aksoy et al., 2008). Despite this, results obtained through the UKIH method are less realistic. Streamflow and baseflow always change gradually under natural conditions. Due to linear interpolation, the baseflow hydrograph obtained from the UKIH methods contains numerous sharp peaks, sharp turns, and troughs contrary to actual conditions (Aksoy, 2008). Moreover, this method is not sensitive to watershed characteristics (Nathan and McMahon, 1990).

3.2.1.2 HYSEP (1996) method

In a hydrograph-separation (HYSEP) method, the time gap used for a target watershed is determined by the following equation:

$$N = A^{0.2} \tag{4}$$

where N is the number of days after which surface runoff ceases, and A is the watershed area in square miles. The interval used for hydrograph separation is specified to be an odd integer between 3 and 11 nearest to 2N. To improve the accuracy at the beginning and end of separation, hydrograph separation begins one interval prior to the start of the separation date and ends one interval after the end of the selected date. Using the ACW area of 79 km^2, the time interval is calculated to be five days.

HYSEP approaches are divided into three groups: a) fixed-interval, b) sliding-interval, and c) local-minimum method, which use different criteria to define the relative minimum points.

a. Fixed-interval method

The fixed-interval method assigns the lowest discharge in each interval (I) to all days in that interval, and the assigned values are connected to form the baseflow hydrograph.

b. Sliding-interval method

The sliding-interval method finds the lowest discharge in one half the interval minus 1 day [0.5(I-1) days] before and after the day being considered and assigns it to that day. The assigned values are then connected to define the baseflow hydrograph.

c. Local-minimum method

The local-minimum method inspects the streamflow value of each day to determine if it is the lowest discharge in one half the interval minus 1 day [0.5(I-1) days] before and after the day being considered. The local-minimum points are connected to form the baseflow hydrograph.

Similar to the UKIH method, the HYSEP methods are standardized and systematic, making them suitable for automation in a computer program which is more convenient (Gonzales et al., 2009). Generally, the estimation results might become biased when streamflow data are recorded during extreme weather conditions (Sloto and Crouse, 1996). Moreover, linear interpolation will lead to the occurrences of stiff turns in the estimated baseflow hydrograph, which is not consistent with actual conditions (Aksoy, 2009).

3.2.2 Digital filter methods

In digital filter methods, the principle is to use the signal frequency analysis to separate baseflow and surface runoff (Indarto et al., 2016). Among runoff generation processes, baseflow always responds slowly to precipitation events, whereas surface runoff responds more quickly. Therefore, baseflow is assumed to be the low-frequency part of the streamflow compared to surface runoff treated as the high-frequency component (Indarto et al., 2016). Based on this assumption, various numerical filters have been developed (Lyne and Hollick, 1979; Chapman, 1991; Chapman and Maxwell, 1996; Eckhardt, 2005; Tularam and Ilahee, 2008) to separate streamflow into low-frequency baseflow and high-frequency surface runoff processes. Each of these methods are briefly described below.

3.2.2.1 Lyne and Hollick (1979) method

Lyne and Hollick (1979) developed a systematic method for understanding the dynamic relationships between streamflow and rainfall events. Baseflow is estimated through the application of the digital filter consisting of the following equations:

$$f_k = \alpha \times f_{k-1} + \frac{1+\alpha}{2} \times (y_k - y_{k-1});\ f_k \geq 0 \tag{5}$$

$$b_k = y_k - f_k \tag{6}$$

where f_k is surface runoff at time k, b_k is baseflow at time t, y_k is the original streamflow at time k, and α is the filter parameter with a value between 0 and 1.

The estimation results of the filter are confined to be lower than streamflow to avoid the slow response baseflow to exceed the original streamflow (Equation 6). Nathan and McMahon (1990) applied the Lyne and Hollick (1979) method to 186 catchments in New South Wales with a mean streamflow data record of 17 years. They set the filter parameter

as 0.9, 0.925, and 0.95 and concluded that the optimal value of the filter parameter is 0.925. In this study, the recommended filter parameter value of 0.925 is used.

The Lyne and Hollick (1979) method is a fast, automated, and objective estimation method. Compared with the UKIH method, the Lyne and Hollick (1979) approach is more suitable for low baseflow conditions due to the less variable and relatively low and smooth baseflow results according to Nathan and McMahon (1990).

3.2.2.2 Chapman and Maxwell (1996) method

Chapman (1991) modified the method developed by Lyne and Hollick (1979). He combined Equations 5 and 6 and eliminated y_k (Equations 7~10), to obtain Equation 11:

$$y_k = b_k + f_k;\ y_{k-1} = b_{k-1} + f_{k-1} \tag{7}$$

$$f_k = \alpha \times f_{k-1} + \frac{1+\alpha}{2} \times [(b_k + f_k) - (b_{k-1} + f_{k-1})] \tag{8}$$

$$\frac{1+\alpha}{2} b_k = \frac{1+\alpha}{2} b_{k-1} + \left(1 - \frac{1+\alpha}{2}\right) f_k + \left(\frac{1+\alpha}{2} - \alpha\right) f_k \tag{9}$$

$$b_k = b_{k-1} + (f_k + f_{k-1})(1-\alpha)/(1+\alpha) \tag{10}$$

$$b_k = b_{k-1} \tag{11}$$

Equations 10 and 11 show that when there is no surface runoff, f_k is equal to zero and the value of baseflow would become a constant between precipitation events when there is no surface runoff, which does not correspond with observations. Hence, Chapman (1991) concluded that the Lyne and Hollick (1979) method did not always yield hydrologically plausible results, and Chapman and Maxwell (1996) improved the following equation by converting the equation of the 1991 version to the weighted average of one day's quick flow and the previous day's baseflow:

$$b_k = \frac{3\alpha-1}{3-\alpha} \times b_{k-1} + \frac{1-\alpha}{3-\alpha} \times (y_k + y_{k-1}) \tag{12}$$

where b_k is baseflow at time t, y_k is the original streamflow at time k, and α is the filter parameter.

After applying Equation 12 to the Salmon catchment in Western Australia, Chapman and Maxwell (1996) found that the optimal value of the filter parameter α is 0.95. The precipitation around this area ranges from 600 ~ 1,000 mm/year with ~150 mm/month in spring and autumn, ~50 mm/month in summer, and ~320 mm/month in winter. The Salmon catchment is a perennial catchment with porous material underlying the river, thus it is similar to the ACW, and a parameter α of 0.95 is used in this study.

One significant disadvantage of this method is that the α may change from one precipitation event to another (Chapman and Maxwell, 1996). From the case studies conducted in nine different catchments including the Alloux catchment in Switzerland, the Marcaidh catchment in Scotland, and an unspecified catchment in Toronto, Canada, it has been confirmed that the fitted value of α decreases as the peak runoff rate increases (Chapman and Maxwell, 1996). Therefore, a constant α value for all precipitation events may not describe the actual baseflow changes.

3.2.2.3 FUKIH (2009) method

The Filtered UKIH method is the combination of the UKIH and digital filter methods (Aksoy et al., 2009). The baseflow obtained by the UKIH method is filtered again using the digital filter developed by Lyne and Hollick (1979) (Equations 5, 6) to obtain the final baseflow estimates.

In the UKIH method, the approach merely connects the consecutive turning points through linear interpolation generating numerous sharp peaks and stiff turns, which is not in accordance with actual baseflow changes. That is, it is not hydrologically plausible. In

the filtered UKIH method, these sharp peaks are removed to obtain a smoothed baseflow hydrograph (Aksoy et al., 2009).

Compared to the baseflow hydrograph estimated through the UKIH method, the FUKIH method eliminates sharp peaks and troughs, thus leading to more realistic estimation results, which take the delayed response of baseflow into consideration (Aksoy et al., 2009). However, the performance of the FUKIH method relies heavily on the accuracy of the result of the UKIH method. If the estimated baseflow obtained from the UKIH method is low in accuracy, the performance of the FUKIH method is also affected.

3.2.2.4 Eckhardt (2005) method

Prior to the development of the Eckhardt (2005) method, most recursive filtering methods used for baseflow estimation relied on a single parameter filter. In the Eckhardt (2005) method, two parameters, the filter parameter and the maximum value of baseflow index are used to describe the flow behaviour.

$$b_k = \frac{(1-BFI_{max})ab_{k-1}+(1-a)BFI_{max}y_k}{1-aBFI_{max}} \quad (13)$$

where y_k represents streamflow at time k, b_k represents baseflow at time k, a represents a filter parameter, and BFI_{max} represents the maximum value of the baseflow index (*BFI*), which is the long-term ratio of baseflow to total streamflow.

Eckhardt (2005) discussed that these previous one-parameter filters that described the recession of the baseflow (Chapman and Maxwell, 1996) were special cases of the two-parameter filter. For example, if the BFI_{max} is set to be 0.5, Equation 13 can be simplified into the equation developed by Chapman and Maxwell (1996). If the value of BFI_{max} is set to other values, the estimated baseflow will be different. Therefore, Eckhardt (2005) proposed that a two-parameter filter was necessary to better describe baseflow variations.

For different catchments with different characteristics, each catchment has its own geological and hydrological settings, which lead to different BFI_{max} values. To minimize the subjective effects of the BFI_{max}, setting appropriate values for BFI_{max} and filter parameter based on the type of the watershed is necessary. In the following equations for each kind of catchment, the filter parameter a is the recession constant, which is determined through the construction of a master recession curve using the matching strip method (Nathan and McMahon, 1990). BFI_{max} is defined from previous baseflow estimation studies, which are conducted in watersheds with representative features. Eckhardt (2005) examined several case studies of three kinds of catchments, including perennial streams with porous aquifers, ephemeral streams with porous aquifers, and perennial streams with hard rock aquifers. The formula is simplified into different forms for catchments with diverse geological environments as follows:

- *Perennial streams, porous aquifer catchment*

There are two North American catchments being studied using the data from US Geological Survey for assessing this two-parameter filter— the Brandywine Creek catchment in Pennsylvania, and the Beaverdam Creek catchment in Maryland (Eckhardt, 2005). The BFI_{max} is determined from the study of Arnold and Allen (1999) and has a value of 0.8. When BFI_{max} is set to be 0.8 in perennial streams, porous aquifer catchment, Equation 13 is simplified as below:

$$b_k = \frac{ab_{k-1}+4(1-a)y_k}{5-4a} \tag{14}$$

- *Ephemeral streams, porous aquifer catchment*

The Goose Creek and Hadley Creek catchments in Illinois, USA are considered for catchments with ephemeral streams and porous aquifers (Eckhardt, 2005). The BFI_{max}

determined based on the research by Chapman and Maxwell (1996) is 0.5. When BFI_{max} is set to be 0.5 in ephemeral streams, porous aquifer catchment, Equation 13 is revised as below:

$$b_k = \frac{ab_{k-1}+(1-a)y_k}{2-a} \quad (15)$$

- *Perennial streams, hard rock aquifer catchment*

Three mesoscale catchments located around the low mountain range at the southwest of the Rhenish Massif in Germany are examples for catchments with hard rock aquifers. The BFI_{max} is 0.25 through the study of Kaviany (1978). When BFI_{max} is set to be 0.25 in perennial streams, hard rock aquifer catchment, Equation 13 is revised as below:

$$b_k = \frac{3ab_{k-1}+(1-a)y_k}{4-a} \quad (16)$$

Considering the hydrological condition and the surficial material at the ACW, the ACW is a catchment with a perennial stream. Therefore, the BFI_{max} value used in this study is selected to be 0.8, respectively.

According to Xie et al. (2020), reliable baseflow estimation results could be obtained by the Eckhardt (2005) method after the performances of several estimation approaches are assessed through the comparison of estimated baseflow and the true baseflow determined through the approach developed by Xie et al. (2020). In the Eckhardt (2005) method, two parameters are used which may better describe the baseflow changes in different hydrologic and geologic environments.

3.2.2.5 Furey and Gupta (2001) method

Furey and Gupta (2001) considered that previous baseflow estimation methods were simply built based on the assumption that surface runoff and baseflow were treated as high- and low-frequency signals, respectively. However, Furey and Gupta (2001) mentioned the

work conducted by Spongberg (2000) who used a Fourier frequency analysis to show that there were still low-frequency variations embedded in overland flow which would be mistakenly confused with baseflow, thus baseflow might be overestimated leading to inaccurate baseflow estimates. Therefore, Furey and Gupta (2001) developed an approach based on mass balance equation. However, a disadvantage of this approach is that there are no constraints on values of baseflow estimates allowing for baseflow to be larger than streamflow.

$$\bar{Q}_{B,J} = (1-\gamma)\bar{Q}_{B,J-1} + \gamma\left(\frac{c_3}{c_1}\right)\left(\bar{Y}_{B,J-d-1} - \bar{Q}_{B,J-d-1}\right) \tag{17}$$

$$c_3 + c_2 + c_1 = 1 \tag{18}$$

$$\gamma \equiv \beta s \tag{19}$$

$$\beta = \left(\frac{3KbA}{S_y a^2}\right) \tag{20}$$

where $\bar{Q}_{B,J}$ is the baseflow for a basin at time *J*, $\bar{Y}_{B,J}$ is streamflow at time *J*, c_1 is overland flow coefficient, c_2 is evapotranspiration coefficient, c_3 is groundwater recharge coefficient, *d* is delay time (i.e., precipitation at time *j* produces overland flow at time *j* and groundwater recharge at time *j*+*d*), S_y is specific yield, *K* is saturated hydraulic conductivity, *b* is mean saturated aquifer thickness, *A* is hillside area, *a* is hillside width, and *s* is the time interval.

The equations are simplified as following:

$$\bar{Q}_{B,J} = (1-\gamma)\bar{Q}_{B,J-1} + \gamma\left(\frac{c_3}{c_1}\right)\left(\bar{Y}_{B,J} - \bar{Q}_{B,J}\right) \tag{21}$$

$$\gamma = 1 - \frac{\bar{Y}_{B,J}}{\bar{Y}_{B,J-1}},\ \bar{P}_{B,J} = \bar{P}_{B,J-1} = \bar{P}_{B,J-d-1} = 0 \tag{22}$$

$$c_1 = \frac{\bar{Y}_{B,J} - (1-\gamma)\bar{Y}_{B,J-1}}{\bar{P}_{B,J}},\ \bar{P}_{B,J} > 0,\ \bar{P}_{B,J-1} = \bar{P}_{B,J-d-1} = 0 \tag{23}$$

$$c_2 = 1 - \frac{\sum_{J=J_0}^{J_0+T} \bar{Y}_{B,J}}{\sum_{J=J_0}^{J_0+T} \bar{P}_{B,J}} \quad (24)$$

where $\bar{Q}_{B,J}$ is the baseflow for a basin at time J, $\bar{Y}_{B,J}$ is the streamflow at time J, c_1 is overland flow coefficient, c_2 is evapotranspiration coefficient, and c_3 is groundwater recharge coefficient. c_3 is determined based on Equation 18.

To calculate the value of $c_1$and γ, all 2-day periods in a streamflow record during which there is no measured rainfall ($\bar{P}_{B,J} = \bar{P}_{B,J-1} = \bar{P}_{B,J-d-1} = 0$) and periods impacted by rainfall ($\bar{P}_{B,J} > 0$, $\bar{P}_{B,J-1} = \bar{P}_{B,J-d-1} = 0$) are identified, and the number of days since the last rainfall event is also identified for each remaining 2-day period. In order to eliminate the effect of rainfall, when the number of days is larger than 10, the data from these 2-day periods would be used for calculation.

The main advantage of the Furey and Gupta (2001) method is the consideration for low-frequency variations in overland flow that are not lumped with baseflow. However, in this method, if the precipitation data is not accurate enough, the estimates of c_1, c_2, c_3 may also have low accuracy. Moreover, this filter is applied without any calibration and constraints so that baseflow can be overestimated after rainfall events (Furey and Gupta, 2001).

3.2.2.5 EWMA (2008) method

In the Exponentially Weighted Moving Average (EWMA) method, one assumes that the rate of increase of baseflow depends on the fraction of surface runoff (Tularam and Ilahee, 2008). The approach estimates surface runoff at every rise in the hydrograph.

$$B_i = B_{i-1} + \alpha A_i \quad (25)$$

$$B_i = \alpha Y_i + (1 - \alpha) B_{i-1} \quad (26)$$

where B_i is baseflow at time i, A_i is surface runoff at time i, α is the fraction of surface runoff, Y_i is stream flow at time i.

In this method, Tularam and Ilahee (2008) considered four case studies conducted at the Bremer River and Tenhill Creek catchments in Queensland, Australia. In these catchments, the geological material underlying beneath the river is a highly permeable basalt. The annual precipitation is ~1,000 mm/year with ~100 mm/month in spring, ~40 mm/month in summer, and ~150 mm/month in winter, which is similar to the ACW. Moreover, the optimal baseflow estimation coefficient is selected for each catchment through several trial-and-error analysis without incurring much computational cost. Consequently, the optimal estimation coefficient α of 0.013 is used in this study.

The potential disadvantage is that in the EWMA (2008) method, a single α value may not yield acceptable baseflow estimation results for all precipitation events (Tularam and Ilahee, 2008). That is, the optimal parameter value may vary from event to event. However, it is found that the estimated baseflow does not show extreme sensitivity to a change in α. Tularam and Ilahee (2008) mentioned that it has been found that a 50% change in α would lead to less than 10% variation in the estimation results, which is within acceptable limits. Therefore, when using this method, a single α value is still used for the calculation of baseflow.

Chapter 4

Evaluation of baseflow estimation methods with actual data

Figure 5 shows the baseflow estimated using actual streamflow data at the New Dundee gauging station through four graphical estimation methods and six digital filter methods, while Table 1 summarizes the arithmetic mean, maximum, and minimum values of the baseflow estimated from each estimation approach. Table 1 shows that the arithmetic mean values range from 0.082 to 0.186 m^3/s, and the mean values from the UKIH and FUKIH approaches are relatively lower than other approaches. The maximum baseflow values range from 0.262 to 1.840 m^3/s, and the FUKIH approach generates the lowest maximum values. As for the minimum values, all baseflow estimation approaches generate a same minimum value of 0.003 m^3/s except for the Furey and Gupta approach. The arithmetic mean, maximum, and minimum values from the Furey and Gupta approach are all largest throughout the ten estimation approaches. Generally, baseflow estimates generated from the FUKIH approach are lower, whereas baseflow estimates from the Furey and Gupta approach are higher.

Due to the lack of actual baseflow data, the estimated baseflow results can only be analyzed based on hydrologic plausibility (Nathan and McMahon, 1990), which means to evaluate the rationality of the estimated values and to investigate whether the features of the resulted baseflow correspond with those that result in natural environment or not, such as whether the observed baseflow shows delayed response to precipitation and whether baseflow shows an unusual increased amount and increasing/decreasing rate during rainfall.

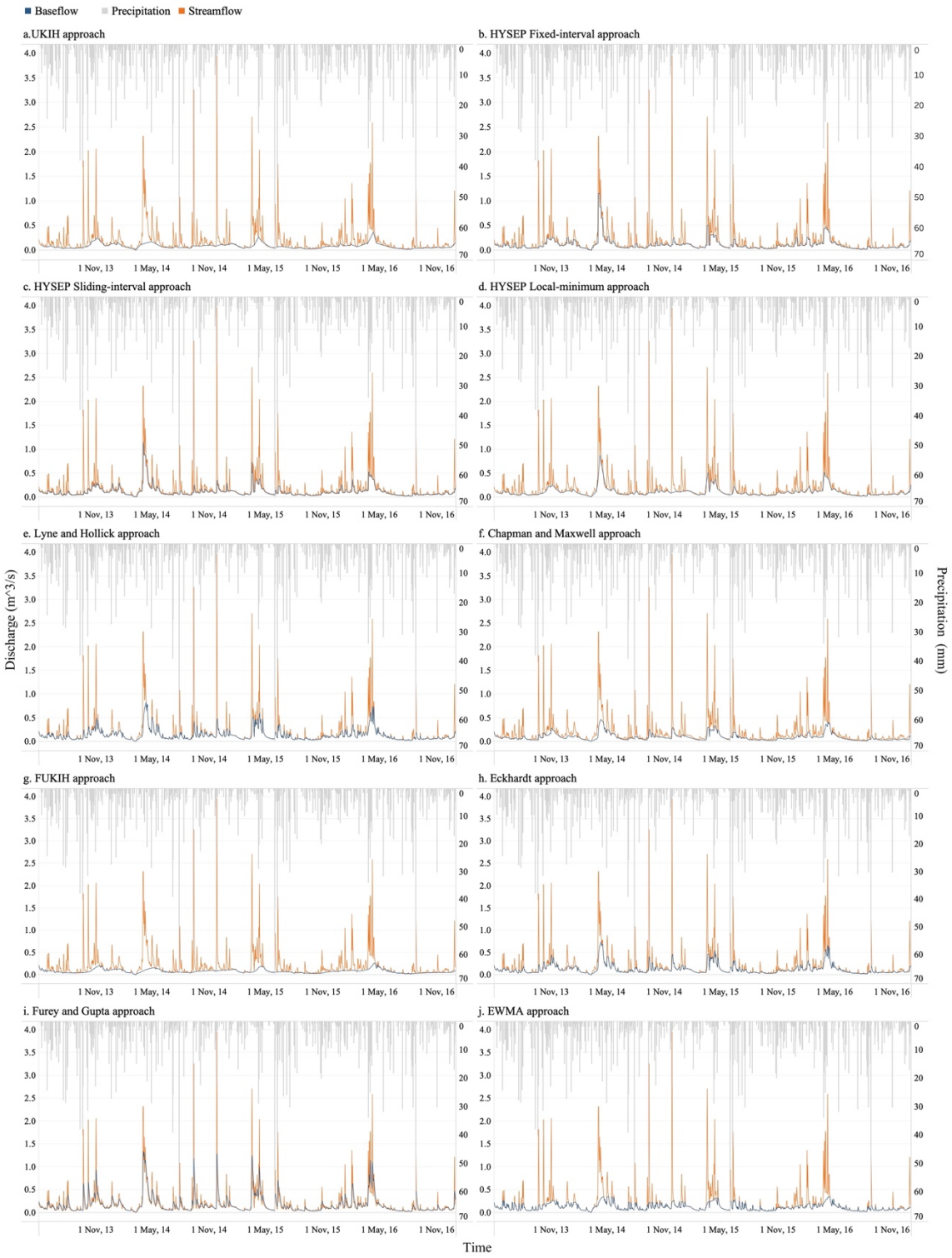

Figure 5. Streamflow records over the period of May 2013 – Dec 2016 at the New Dundee gauging station and corresponding baseflow estimated through the: a) UKIH; b) HYSEP-Fixed interval; c) HYSEP-Sliding interval; d) HYSEP-Local minimum; e) Lyne and Hollick; f) Chapman and Maxwell; g) FUKIH; h) Eckhardt; i) Furey and Gupta; and j) EWMA approaches. Precipitation records are from the Roseville station.

Table 1. Mean, maximum, and minimum values of baseflow estimated using actual streamflow data through ten different estimation approaches at the New Dundee gauging station.

Baseflow estimation results with actual data at the New Dundee gauging station			Mean	Maximum	Minimum
			(m^3/s)		
Graphical method	UKIH method		0.084	0.436	0.003
	HYSEP	Fixed-interval	0.110	1.150	0.003
		Sliding-interval	0.108	1.150	0.003
		Local-minimum	0.106	0.879	0.003
Digital filter method	Lyne and Hollick method		0.141	0.824	0.003
	Chapman and Maxwell method		0.098	0.463	0.003
	FUKIH method		0.082	0.262	0.003
	Eckhardt method		0.133	0.731	0.003
	Furey and Gupta method		0.186	1.840	0.006
	EWMA method		0.125	0.350	0.003

From Figure 5, it is shown that the baseflow hydrograph from the UKIH approach (Figure 5a) is flat and does not show an obvious change during precipitation events. In the HYSEP fixed-interval method (Figure 5b), the change of baseflow is more distinct than that in the UKIH approach. During precipitation, baseflow increases significantly over a short duration. In particular, it reveals a staircase pattern, which does not correspond with natural conditions.

Comparing between these three HYSEP approaches (Figure 5b-d), all these three approaches generate a large increase in baseflow during rainfall events, and the changing trend of estimated baseflow in the HYSEP sliding-interval approach is similar to that in the fixed-interval approach. In the HYSEP approaches, large increases of baseflow and the staircase pattern could be observed during rainfall events, which does not correspond with the delayed increase of baseflow expected under actual conditions. Furthermore, due to the linear interpolation used in graphical approaches, the hydrograph of the HYSEP local-minimum approach (Figure 5d) contains numerous shark peaks and stiff turns, which appears to be abnormal.

For the digital filter approaches, the overall changes of baseflow are much smoother than those from the graphical approaches. For example, in the Lyne and Hollick approach (Figure 5e), although the increased amount of baseflow is not as large as that in the HYSEP sliding-interval approach (Figure 5c), it still shows a significant increase during some precipitation events, which is similar to results from the HYSEP local-minimum approach (Figure 5d). In the Chapman and Maxwell approach (Figure 5f), the change of the baseflow is smoother than that in Lyne and Hollick approach (Figure 5e), and the increase during precipitation is also lower. In the FUKIH approach (Figure 5g), as mentioned before, baseflow is first calculated by the UKIH graphical approach, and then filtered and smoothed by a digital filter, thus leading to an extremely flat baseflow hydrograph without obvious changes throughout the year. As for the Eckhardt approach (Figure 5h), large increases during precipitation are also observed, and the amount of increase is similar to that in the Lyne and Hollick approach (Figure 5e). For the Furey and Gupta approach (Figure 5i), as introduced in the methods part, there is no constraint set for baseflow, hence the baseflow values sometimes become larger than streamflow. Except for this anomaly, the response of baseflow to precipitation is extraordinarily quick together with large baseflow increase values, which is inconsistent with the anticipated slow response characteristic of baseflow.

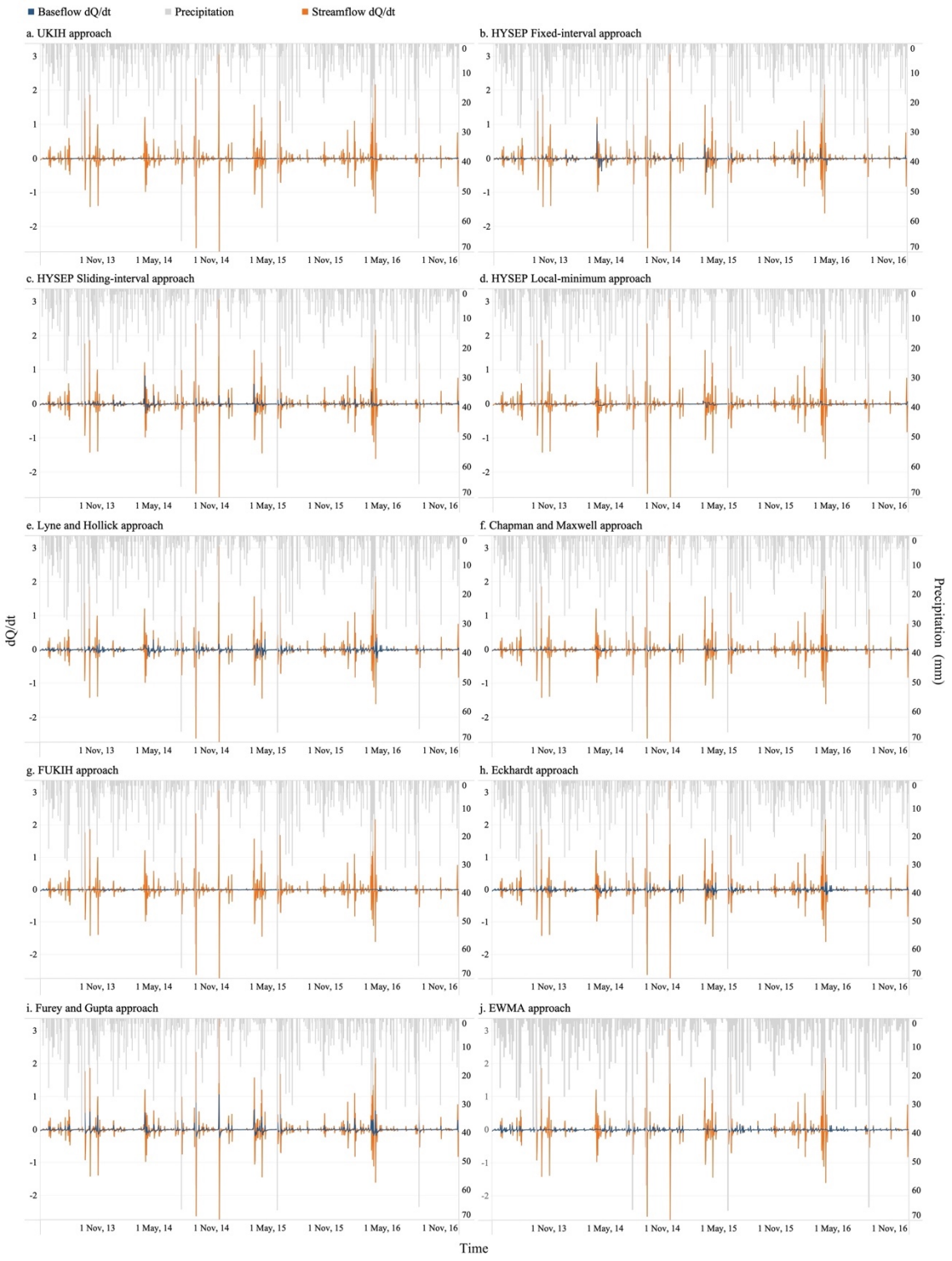

Figure 6. Time derivative of flow rate with respect to time (dQ/dt) of streamflow and baseflow at the New Dundee gauging station. Baseflow results are calculated through the: a) UKIH; b) HYSEP-Fixed interval; c) HYSEP-Sliding interval; d) HYSEP-Local minimum; e) Lyne and Hollick; f) Chapman and Maxwell; g) FUKIH; h) Eckhardt; i) Furey and Gupta; and j) EWMA approaches.

In order to better quantify the change of baseflow with time and to examine the hydrologic plausibility of various baseflow estimation techniques, the discharge derivative with respect to time (dQ/dt) is obtained by calculating the change of discharge within each day based on the baseflow and streamflow data obtained through ten different techniques. According to Nathan and McMahon (1990), the use of dQ/dt in conjunction with streamflow and baseflow hydrographs may be able to better identify rates of increase or decrease and assess the hydrologic plausibility of each baseflow estimation technique, and then help select the most optimal technique.

Figure 6 shows the resulting dQ/dt estimates for these ten approaches to visualize the change in discharge of both streamflow and baseflow with time. Examination of results reveals that for the HYSEP fixed-interval approach (Figure 6b), the dQ/dt of baseflow is very large during precipitation and is almost the same as the dQ/dt of streamflow during some precipitation events. This abnormally large dQ/dt of baseflow is not only observed in the HYSEP fixed-interval approach (Figure 6b), but also shown in the HYSEP sliding-interval (Figure 6c) and Furey and Gupta (Figure 6i) approaches.

Combining the baseflow derivative analyses with previous baseflow hydrograph analyses, baseflow values estimated through all these four graphical approaches (Figures 6a-d) show relatively large increases during precipitation events, and the baseflow hydrographs are not smooth, especially for the staircase patterns shown in the hydrographs of the HYSEP fixed (Figure 6b) and sliding-interval (Figure 6c) approaches. Also, the baseflow estimates from these approaches increase dramatically during precipitation events. A large increase of baseflow during precipitation is observed, not only in graphical approaches, but also in the Furey and Gupta approach (Figure 6i). For the results obtained

from the Lyne and Hollick (Figure 6e) and Eckhardt approaches (Figure 6h), the increase during precipitation is also very obvious. Based on the derivative analysis, baseflow estimation results obtained from these approaches may not be treated as hydrologically plausible results.

However, although some of the baseflow estimation approaches generate baseflow estimates that are not hydrologically plausible, it is still difficult to determine the most optimal approach based on the analyses of hydrographs or its derivatives alone. This is because data on true baseflow from the ACW is lacking, and the criteria utilized to determine whether the given baseflow estimation approach is hydrologically plausible or not is subjective. Therefore, further assessment of baseflow estimation techniques through simulated results from a 3D integrated hydrologic model is necessary. In particular, baseflow values estimated through these ten baseflow estimation techniques are compared with the synthetic baseflow obtained from the HGS model to evaluate the performances of different approaches in the next section.

Chapter 5

Evaluation of baseflow estimation methods with synthetic data

5.1 Synthetic baseflow simulated from the HGS model

In this study, synthetic streamflow and baseflow at ten different study points from May 1st, 2013 to April 30th, 2016 are obtained from the HGS model of the ACW constructed by Tong et al (2022). As introduced in the introduction part, although this HGS model could not generate the streamflow and baseflow estimates that are thoroughly same as true

streamflow and baseflow values, the model is still of good performance, thus leading to simulation results that are reliable enough to be used to describe the flow conditions at the ACW and investigate the performance of baseflow estimation techniques. Figure 7 shows the comparison between synthetic streamflow and actual streamflow from May 1st, 2013 to April 30th, 2016. From this figure, it could be observed that although actual streamflow and synthetic streamflow are not perfectly the same, these two kinds of streamflow are close to each other during most of the time, and the amount of increase during precipitation is also similar. Therefore, synthetic streamflow is utilized to estimate the baseflow through the ten baseflow estimation approaches utilized earlier, and synthetic baseflow obtained from the model could be treated as true baseflow to help determine the performance of different estimation approaches.

Figure 8 shows the comparison between synthetic streamflow and baseflow obtained from the HGS model, as well as estimated baseflow calculated based on synthetic streamflow at the New Dundee gauging station (Point 7). The synthetic baseflow obtained from the HGS model is relatively low throughout the year and does not show an obvious increase during precipitation. In general, the synthetic baseflow hydrograph from HGS is smoother and there are no sharp peaks observed.

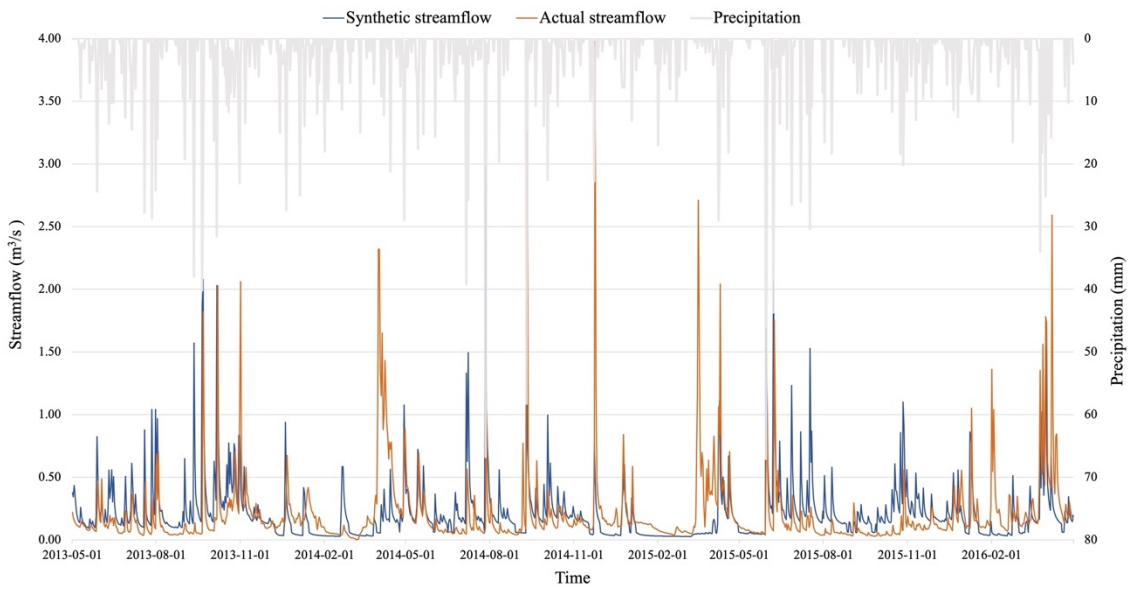

Figure 7. Comparison between actual streamflow and synthetic streamflow from May 1st, 2013 to April 30th, 2016.

Compared with synthetic baseflow, estimated baseflow calculated through the Furey and Gupta approach shows abnormally high values (Figure 8i). Baseflow estimated through the Eckhardt (Figure 8h) and Lyne and Hollick (Figure 8e) approaches are also obviously higher than synthetic baseflow. Compared with the estimated baseflow obtained through these three estimation techniques, the baseflow from the remaining seven approaches (Figure 8a-d; 8f-g; 8j) is lower and closer to synthetic baseflow.

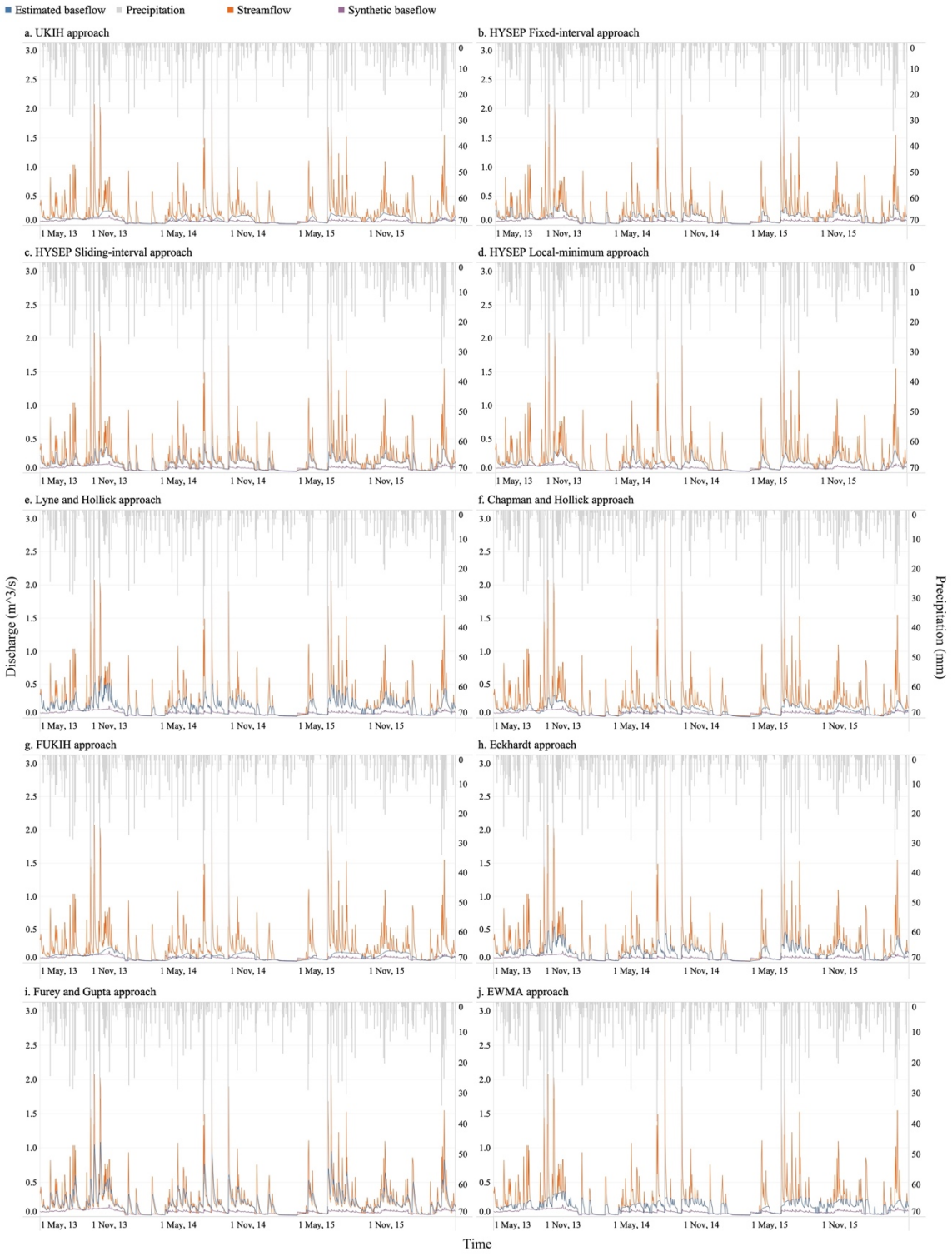

Figure 8. Comparison between synthetic baseflow obtained from the HGS model and estimated baseflow at Point 7 calculated through the: a) UKIH; b) HYSEP-Fixed interval; c) HYSEP-Sliding interval; d) HYSEP-Local minimum; e) Lyne and Hollick; f) Chapman and Maxwell; g) FUKIH; h) Eckhardt; i) Furey and Gupta; and j) EWMA approaches.

However, baseflow hydrographs estimated through three HYSEP approaches (Figure 8b-d), the Chapman and Maxwell approach (Figure 8f), and the EWMA approach (Figure 8j) are not flat and show obvious increases during precipitation, which does not correspond to the synthetic baseflow hydrographs from HGS. Overall, the estimated baseflow hydrographs obtained through the UKIH (Figure 8a) and FUKIH (Figure 8g) approaches are far lower and flatter than the baseflow hydrographs from the other baseflow estimation approaches. In order to quantitatively determine which estimation approach results in baseflow hydrographs most similar to the synthetic baseflow hydrograph, model performance statistics are computed and discussed in the next section.

5.2 Performance assessment of baseflow estimation techniques

Figure 9 shows the scatterplots between synthetic and estimated baseflow for ten different baseflow estimation techniques at the New Dundee gauging station (Point 7). Scatterplots for the other points are provided in the Appendix as Figures A10 – A18. The red dashed regression lines and the corresponding equations show the relationship between the synthetic and estimated baseflow. The solid black lines 1:1 lines indicate a perfect fit. The coefficient of determination (R^2) shown in each graph represents how well the regression line approximates the original baseflow data. The L_1 norm is the mean absolute error, which measures the absolute difference between synthetic and estimated baseflow, while the L_2 norm is the mean squared error, which measures the average squared difference between baseflow estimates and synthetic baseflow. The smaller the L_1 and L_2 norms, the higher the correspondence of the synthetic and estimated baseflow, and the better the performance of the estimation approach.

The R^2 value as well as L_1 and L_2 norms are calculated as:

$$R^2 = 1 - \frac{RSS}{TSS} \tag{28}$$

$$RSS = \sum_i^n (Q_m^t - \widehat{Q_m^t})^2 \tag{29}$$

$$TSS = \sum_i^n (Q_m^t - \overline{Q_m})^2 \tag{30}$$

$$L_1(Q_m, Q_0) = \frac{1}{N}\sum_t^n |Q_m^t - Q_0^t| \tag{31}$$

$$L_2(Q_m, Q_0) = \frac{1}{N}\sum_t^n (Q_m^t - Q_0^t)^2 \tag{32}$$

where *RSS* is sum of squares of residuals, *TSS* is total sum of squares. Q_m^t is the estimated baseflow at time *t*, Q_0^t is synthetic baseflow at time *t*, and *N* is the total number of baseflow values. $\widehat{Q_m^t}$ is the corresponding predicted value of Q_m^t located on the line of best fit, $\overline{Q_m}$ is the average value of estimated baseflow.

As mentioned previously, the synthetic baseflow obtained from the HGS model is relatively low throughout the year, and the estimated baseflow is normally higher than synthetic baseflow resulting in a significant bias on Figure 8. During dry seasons, both estimated baseflow and synthetic baseflow are close to streamflow, but during precipitation events, estimated baseflow is obviously higher than synthetic baseflow. The scatterplots also reveal this feature (Figure 9), especially for the Furey and Gupta approach where the estimated baseflow is significantly higher than synthetic baseflow (Figure 9i). From the regression lines in Figure 9, the regression line slopes of the UKIH (Figure 9a) and the FUKIH (Figure 9g) are closer to the 1:1 line than the other approaches, which indicates that the similarity of estimated and synthetic baseflow is higher when using the UKIH (Figure 9a) and FUKIH (Figure 9g) approaches.

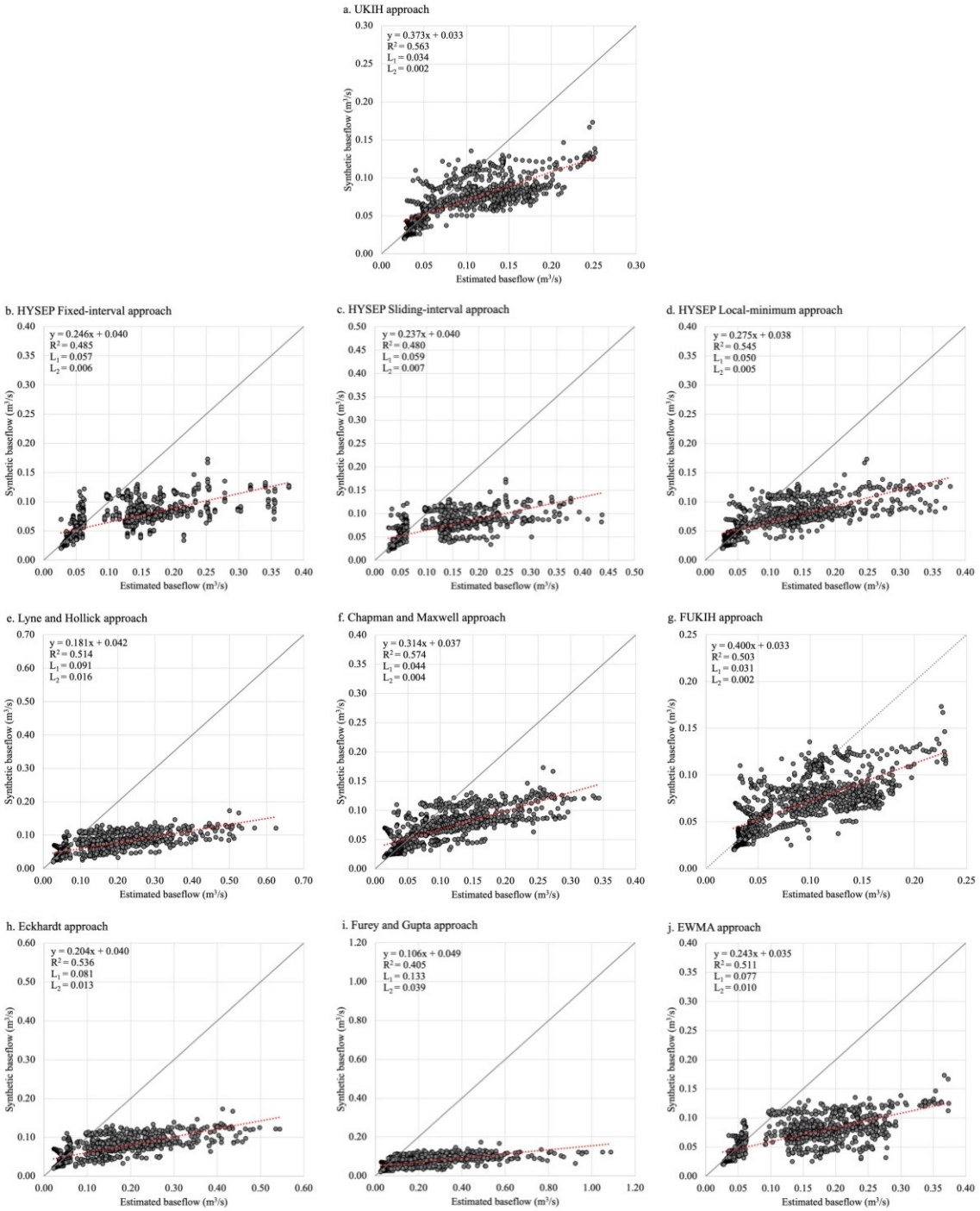

Figure 9. Scatter plots showing the relationship between synthetic baseflow obtained from the HGS model and estimated baseflow at Point 7 calculated through the: a) UKIH; b) HYSEP-Fixed interval; c) HYSEP-Sliding interval; d) HYSEP-Local minimum; e) Lyne and Hollick; f) Chapman and Maxwell; g) FUKIH; h) Eckhardt; i) Furey and Gupta; and j) EWMA approaches. The dashed red lines are the regression lines, while the solid black lines are the 1:1 lines describing a perfect fit.

Table 2. Slope, intercept, and R^2 of baseflow regression line at the ten study points. The maximum slope, minimum intercept, and maximum R^2 are assigned a color of dark green, the minimum slope, maximum intercept, and minimum R^2 is assigned a color of dark red. Bold numbers indicate the best result among all the approaches.

Ten baseflow estimation approaches		UKIH	HYSEP FI	HYSEP SI	HYSEP LM	LH	CM	FUKIH	Eckhardt	FG	EWMA
slope	Point 1	0.590	0.579	0.579	0.593	0.555	**1.074**	0.591	0.677	0.571	0.701
intercept		0.007	0.007	0.007	0.007	0.008	0.007	0.008	0.007	0.008	**0.005**
R^2		0.747	0.734	0.734	0.754	0.732	0.697	0.714	0.727	0.726	**0.782**
slope	Point 2	0.162	0.055	0.056	0.096	0.056	0.101	**0.214**	0.063	0.030	0.090
intercept		0.017	0.022	0.022	0.020	0.020	0.019	**0.015**	0.020	0.022	0.018
R^2		0.161	0.063	0.068	0.125	0.104	0.119	**0.179**	0.109	0.074	0.131
slope	Point 3	0.509	0.303	0.308	0.368	0.249	0.410	**0.698**	0.280	0.127	0.385
intercept		0.005	0.025	0.024	0.021	0.025	0.023	**0.001**	0.024	0.036	0.013
R^2		0.594	0.333	0.355	0.421	0.386	0.370	**0.624**	0.394	0.233	0.490
slope	Point 4	0.517	0.240	0.244	0.297	0.196	0.327	**0.597**	0.223	0.108	0.304
intercept		0.013	0.052	0.051	0.044	0.053	0.048	**0.006**	0.050	0.069	0.033
R^2		0.553	0.290	0.302	0.373	0.323	0.318	**0.606**	0.335	0.210	0.422
slope	Point 5	0.528	0.242	0.252	0.310	0.214	0.367	**0.625**	0.250	0.127	0.322
intercept		**0.002**	0.045	0.043	0.035	0.043	0.038	0.009	0.039	0.060	0.022
R^2		0.555	0.287	0.309	0.381	0.342	0.333	**0.616**	0.360	0.233	0.427
slope	Point 6	0.530	0.517	0.520	0.494	0.509	**0.868**	0.500	0.644	0.562	0.538
intercept		**0.023**	0.025	0.024	0.027	0.025	0.031	0.027	**0.023**	**0.023**	0.024
R^2		0.641	0.605	0.624	0.598	0.630	0.490	0.563	0.607	**0.663**	0.592
slope	Point 7	0.373	0.246	0.237	0.275	0.181	0.314	**0.400**	0.204	0.106	0.243
intercept		**0.033**	0.040	0.040	0.038	0.042	0.037	**0.033**	0.040	0.049	0.035
R^2		0.563	0.485	0.480	0.545	0.514	**0.574**	0.503	0.536	0.405	0.511
slope	Point 8	0.637	0.400	0.405	0.451	0.312	0.504	**0.700**	0.356	0.197	0.421
intercept		0.045	0.098	0.096	0.088	0.110	0.110	**0.034**	0.105	0.140	0.081
R^2		0.791	0.632	0.646	0.698	0.650	0.652	**0.829**	0.675	0.499	0.720
slope	Point 9	0.525	0.273	0.286	0.319	0.272	0.471	**0.618**	0.328	0.179	0.394
intercept		0.090	0.202	0.196	0.183	0.188	0.184	**0.054**	0.174	0.238	0.126
R^2		0.660	0.437	0.466	0.511	0.539	0.503	**0.771**	0.568	0.388	0.644
slope	Point 10	0.521	0.239	0.242	0.315	0.224	0.370	**0.617**	0.263	0.125	0.345
intercept		0.092	0.243	0.241	0.204	0.236	0.235	**0.047**	0.225	0.300	0.161
R^2		0.629	0.379	0.395	0.470	0.462	0.435	**0.727**	0.481	0.300	0.581

Table 3. L_1 and L_2 norms of estimated vs. simulated baseflow at the ten study points. The minimum L_1 and L_2 norms are assigned a color of dark green, the maximum L_1 and L_2 norms are assigned a color of dark red. Bold numbers indicate the best result among all the approaches.

Ten baseflow estimation approaches		UKIH	HYSEP FI	HYSEP SI	HYSEP LM	LH	CM	FUKIH	Eckhardt	FG	EWMA
L_1	Point 1	1.58E-02	1.55E-02	1.55E-02	1.52E-02	1.58E-02	1.03E-02	1.43E-02	1.03E-02	1.53E-02	**9.64E-03**
L_2		4.92E-04	4.10E-04	4.08E-04	3.85E-04	4.39E-04	**1.74E-04**	4.75E-04	1.86E-04	4.13E-04	1.81E-04
L_1	Point 2	3.50E-02	5.84E-02	5.79E-02	4.54E-02	8.14E-02	5.01E-02	**3.02E-02**	7.46E-02	1.18E-01	6.84E-02
L_2		2.26E-03	7.48E-03	7.56E-03	4.55E-03	1.32E-02	4.52E-03	**1.54E-03**	1.08E-02	3.06E-02	7.67E-03
L_1	Point 3	2.73E-02	4.23E-02	4.22E-02	3.64E-02	6.12E-02	2.81E-02	**2.43E-02**	5.35E-02	8.58E-02	5.19E-02
L_2		1.13E-03	3.44E-03	3.45E-03	2.57E-03	6.68E-03	1.49E-03	**8.49E-04**	5.12E-03	1.58E-02	3.91E-03
L_1	Point 4	6.82E-02	1.04E-01	1.03E-01	9.13E-02	1.45E-01	7.13E-02	**5.92E-02**	1.28E-01	1.98E-01	1.24E-01
L_2		7.14E-03	2.08E-02	2.06E-02	1.59E-02	3.83E-02	9.36E-03	**5.27E-03**	2.96E-02	8.14E-02	2.32E-02
L_1	Point 5	8.20E-02	1.17E-01	1.16E-01	1.05E-01	1.55E-01	**7.20E-02**	7.26E-02	1.36E-01	1.99E-01	1.38E-01
L_2		8.93E-03	2.25E-02	2.20E-02	1.73E-02	3.75E-02	8.36E-03	**6.76E-03**	2.82E-02	6.99E-02	2.48E-02
L_1	Point 6	2.36E-02	2.35E-02	2.35E-02	2.27E-02	2.42E-02	2.44E-02	2.21E-02	**8.33E-03**	1.77E-02	2.14E-02
L_2		7.26E-04	7.18E-04	7.18E-04	6.81E-04	7.57E-04	7.12E-04	6.60E-04	**1.73E-04**	4.66E-04	6.26E-04
L_1	Point 7	3.41E-02	5.65E-02	5.89E-02	5.05E-02	9.14E-02	4.41E-02	**3.06E-02**	8.13E-02	1.33E-01	7.72E-02
L_2		2.35E-03	6.40E-03	7.04E-03	5.33E-03	1.61E-02	3.77E-03	**1.82E-03**	1.26E-02	3.95E-02	9.78E-03
L_1	Point 8	4.95E-02	7.37E-02	7.36E-02	6.54E-02	1.14E-01	5.09E-02	**4.32E-02**	9.09E-02	1.54E-01	9.92E-02
L_2		4.23E-03	1.24E-02	1.23E-02	9.70E-03	2.80E-02	4.10E-03	**3.21E-03**	1.85E-02	6.13E-02	1.68E-02
L_1	Point 9	1.49E-01	2.06E-01	2.02E-01	1.84E-01	2.59E-01	**7.18E-02**	1.32E-01	1.99E-01	3.02E-01	2.26E-01
L_2		2.85E-02	6.88E-02	6.59E-02	5.42E-02	9.82E-02	**7.86E-03**	2.12E-02	5.97E-02	1.55E-01	6.45E-02
L_1	Point 10	1.93E-01	2.66E-01	2.63E-01	2.28E-01	3.42E-01	**1.10E-01**	1.73E-01	2.75E-01	4.21E-01	2.99E-01
L_2		4.62E-02	1.16E-01	1.14E-01	7.98E-02	1.78E-01	**2.10E-02**	3.52E-02	1.19E-01	3.31E-01	1.15E-01

Table 3 shows that the L_1 and L_2 norms of the UKIH and the FUKIH approaches are also lower than the other approaches. Furthermore, from the scatterplots of other study points provided in the Appendix and the slope values provided in Table 2, the estimated baseflow is still larger than synthetic baseflow for most cases, and the Furey and Gupta approach always reveal lowest similarity as well as largest L_1 and L_2 norms (Table 2-3), whereas the estimation technique that gives the best approximation of baseflow estimates to synthetic baseflow is different from Point 7 at some points. Figures A1-A9 show the comparison between synthetic baseflow obtained from the HGS model and estimated baseflow at the other nine points, and Figures A10-A18 show the relationship between synthetic baseflow obtained from the HGS model and estimated baseflow at the other nine

points. Overall, the estimated baseflow is consistently larger than the simulated baseflow obtained from HGS although at certain points the correspondence is better, such as the high correspondence at Point 1 and the low correspondence at Point 2. These scatterplots reveal that the most optimal approaches vary at different points. For example, Figure A10 shows that the regression line of the Chapman and Maxwell approach (Figure A10f) is closest to the 1:1 best fit line consistently throughout the ten approaches at Point 1, and the L_1 and L_2 norms are also smallest (Table 3).

To further determine whether an estimation approach is the most optimal one, in the following analysis, the correlation between synthetic and estimated baseflow is assessed through the Nash-Sutcliffe (*NSE*) number. The *NSE* number is calculated as following to quantify the goodness of fit between the synthetic and estimated baseflow:

$$NSE = 1 - \frac{\sum_t^n (Q_m^t - Q_0^t)^2}{\sum_t^n (Q_0^t - \overline{Q_0})^2} \tag{33}$$

where Q_m^t is the baseflow estimate at time *t*, Q_0^t is the value of the synthetic baseflow at time *t*, and $\overline{Q_0}$ is the mean value of synthetic baseflow.

The *NSE* number ranges from negative infinity to 1.0. The closer the *NSE* number is to 1.0, the closer the estimated baseflow is to synthetic baseflow, and the better the performance of the estimation approach. When the *NSE* number is equal to 1.0, there is a perfect match of synthetic to estimated baseflow; when the *NSE* number is equal to 0.0, the estimation error variance of that estimation approach is equal to the variance of the synthetic baseflow, which means that the predictions of the estimation approach are accurate as the mean value of synthetic baseflow; when the *NSE* number is negative, the synthetic baseflow is a better predictor than the estimation approach. The lower the *NSE* number, the worse the performance of the baseflow estimation approach.

Table 4. *NSE* numbers for ten baseflow estimation approaches at the ten study points. The maximum *NSE* number is assigned a color of dark green, the minimum *NSE* number is assigned a color of dark red. Bold numbers indicate the best result among all the approaches.

Ten baseflow estimation approaches		UKIH	HYSEP FI	HYSEP SI	HYSEP LM	LH	CM	FUKIH	Eckhardt	FG	EWMA
NSE - baseflow	Point 1	-0.51	-0.26	-0.25	-0.18	-0.34	**0.47**	-0.45	0.43	-0.27	0.44
NSE - baseflow dQ/dt		-0.69	-0.99	-0.8	0.04	-0.28	**0.11**	-1.59	0.09	0.03	-0.09
NSE - baseflow	Point 2	-9.55	-33.87	-34.22	-20.2	-60.51	-20.04	**-6.17**	-49.55	-141.78	-34.76
NSE - baseflow dQ/dt		**-2.04**	-113.57	-168.6	-11.49	-143.24	-17.69	-2.43	-89.67	-294.69	-75.19
NSE - baseflow	Point 3	-0.56	-3.74	-3.75	-2.53	-8.19	-1.05	**-0.17**	-6.05	-20.71	-4.38
NSE - baseflow dQ/dt		-0.07	-11.63	-17.34	-1.51	-17.51	-0.76	**-0.06**	-8.51	-40.84	-8.55
NSE - baseflow	Point 4	-1.55	-6.41	-6.33	-4.66	-12.65	-2.34	**-0.88**	-9.54	-28.04	-7.26
NSE - baseflow dQ/dt		-0.13	-18.54	-25.46	-2.55	-26.63	-1.25	**-0.1**	-13.36	-57.84	-13.91
NSE - baseflow	Point 5	-2.51	-7.84	-7.64	-5.79	-13.7	-2.28	**-1.65**	-10.09	-26.43	-8.75
NSE - baseflow dQ/dt		-0.18	-19.31	-24.6	-2.41	-22.83	-0.75	**-0.12**	-9.91	-41.46	-13.44
NSE - baseflow	Point 6	-4.4	-4.34	-4.33	-4.03	-4.66	-4.29	-3.86	**0.13**	-2.27	-3.59
NSE - baseflow dQ/dt		0.22	-0.97	-1.14	0.28	0.41	0.16	0.27	**0.44**	0.28	0.33
NSE - baseflow	Point 7	-2.12	-7.49	-8.35	-6.08	-20.36	-4	**-1.42**	-15.74	-51.45	-11.98
NSE - baseflow dQ/dt		**-0.2**	-9.92	-16.81	-1.5	-25.81	-2.21	-0.77	-14.6	-56.44	-15.01
NSE - baseflow	Point 8	0.01	-1.89	-1.88	-1.27	-5.55	0.04	**0.25**	-3.33	-13.33	-2.92
NSE - baseflow dQ/dt		**-0.25**	-15.26	-19.87	-2.77	-36.03	-2.03	-0.49	-15.92	-76.16	-21.09
NSE - baseflow	Point 9	-2.94	-8.51	-8.11	-6.49	-12.57	**-0.09**	-1.93	-7.26	-20.48	-7.92
NSE - baseflow dQ/dt		-0.32	-27.46	-32.26	-3.42	-21.5	-0.91	**-0.25**	-5.99	-31.19	-12.84
NSE - baseflow	Point 10	-3.59	-10.48	-10.34	-6.93	-16.67	**-1.09**	-2.5	-10.81	-31.89	-10.4
NSE - baseflow dQ/dt		-0.44	-39.94	-58.27	-3.71	-39.85	-2.89	**-0.3**	-16.09	-78.8	-20.14

Table 4 summarizes the *NSE* numbers for all the baseflow estimation approaches at these ten study points, which measures the similarity of baseflow and dQ/dt between estimated baseflow and synthetic baseflow. As mentioned before, the closer the *NSE* number is to 1.0, the closer the estimated baseflow is to synthetic baseflow, and the better the performance of the estimation approach. Therefore, higher *NSE* number means better results. The good results are marked with dark green and shown in bold, and the poor results are highlighted with red. Table 4 shows that the *NSE* values between synthetic and estimated baseflow obtained through most of estimation approaches are negative, and some of them are significantly small, which represents an unsatisfactory fit with synthetic

baseflow. This is likely due to the differences in the physical and mathematical representation of baseflow by the HGS model and the various graphical estimation approaches. In particular, for the HGS model, detailed information about the catchment environment, including the problem geometry, soil type, land use, as well as surface water and groundwater flow parameters are utilized to build the model and to simulate baseflow values, thus physical processes are more explicitly considered in HGS. In contrast, in graphical and filter approaches, only the streamflow record is utilized to estimate the baseflow values, and some estimation approaches may not be suitable at a given point within the watershed, leading to large differences between synthetic and estimated baseflow, ultimately resulting in negative *NSE* numbers, some of which are unacceptably large. From the results, it is obviously determined that the most optimal approach for Points 2, 3, 4, 5, 7, 8 is the FUKIH approach, the most optimal approach for Points 1, 9, 10 is the Chapman and Maxwell approach, and the most optimal approach for Point 6 is Eckhardt approach.

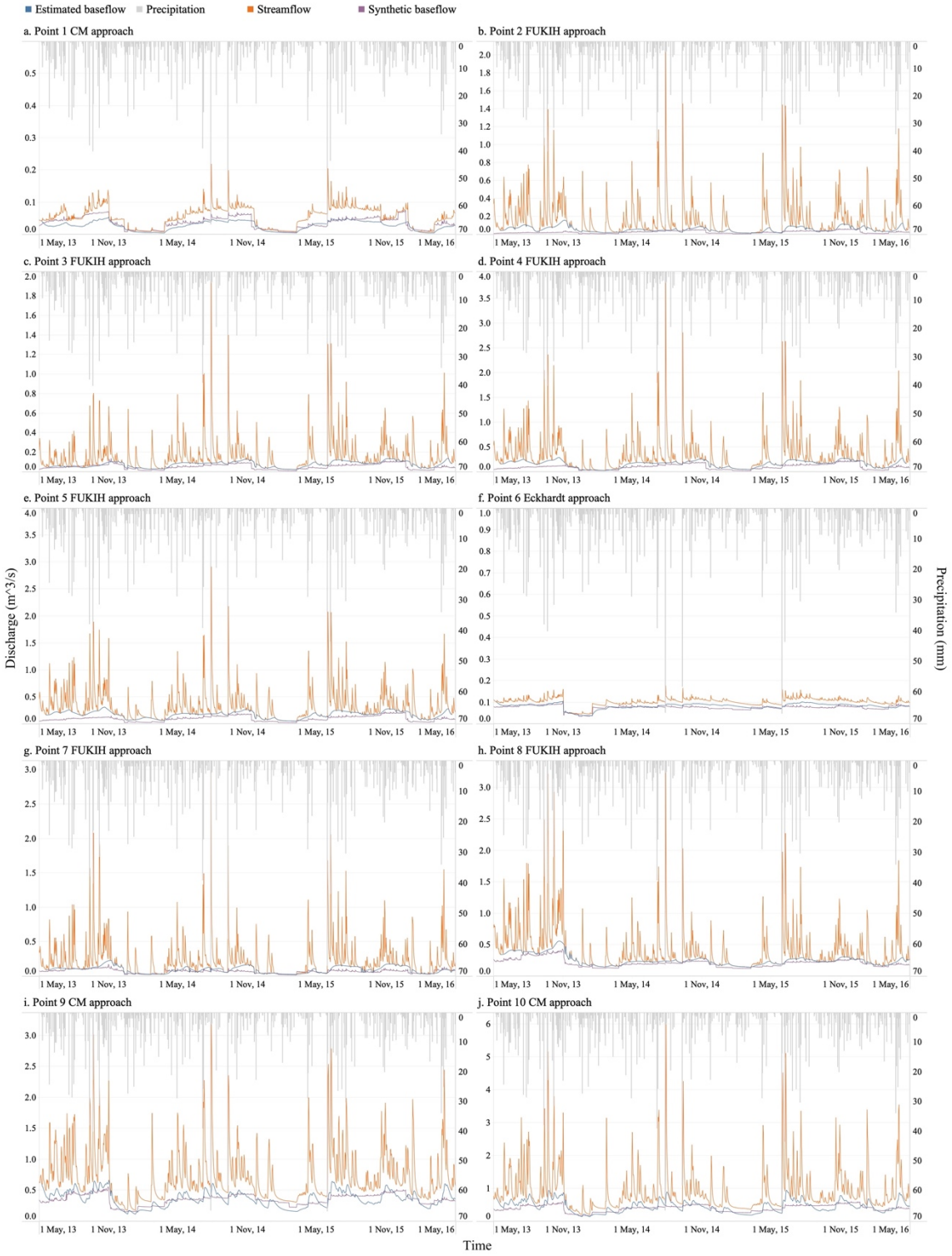

Figure 10. Comparison between synthetic and estimated baseflow calculated through the most optimal approach at: a) point 1; b) point 2; c) point 3; d) point 4; e) point 5; f) point 6; g) point 7; h) point 8; i) point 9; and j) point 10.

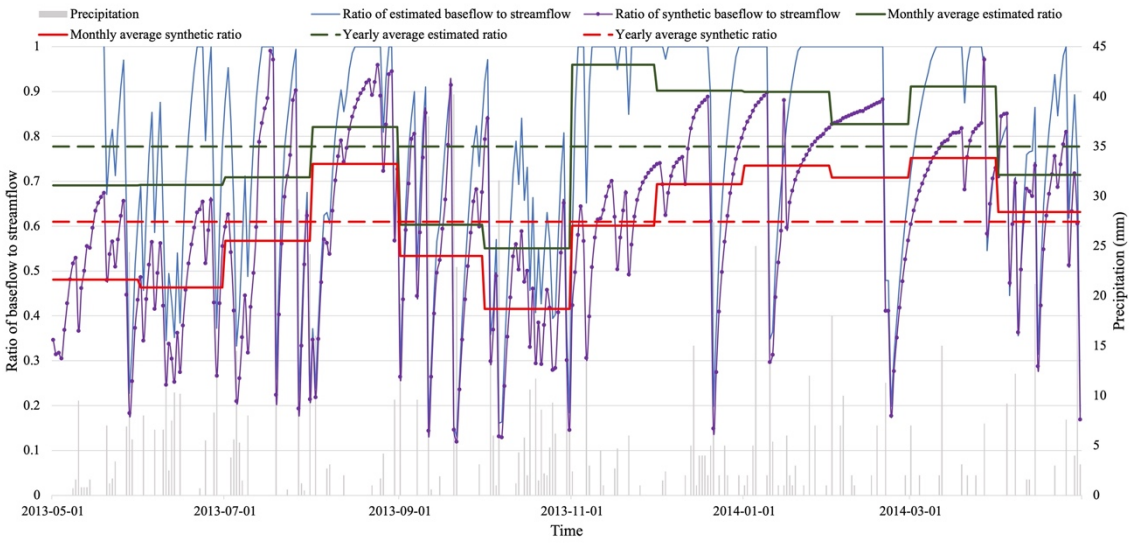

Figure 11. Ratio of estimated baseflow obtained through the FUKIH approach to streamflow and synthetic baseflow to streamflow at point 8 from May 2013 to April 2016. Orange line is the average value of synthetic baseflow; green line is the average value of estimated baseflow.

Figure 11 shows the ratio of estimated baseflow through the FUKIH approach and synthetic baseflow to streamflow at Point 8, as well as its yearly and monthly averages from May 1st, 2013 to April 30th, 2014. It is shown that the ratio of estimated baseflow to streamflow is approximately 0.80 ~ 1.00 when there is almost no precipitation during dry seasons, whereas during precipitation events, baseflow only constitutes a small portion of streamflow. During the time with low precipitation, the monthly average ratio of baseflow to streamflow always become higher. For example, the monthly average ratios for August 2013 and November 2013 are 0.82 and 0.96, higher than the monthly average ratios for the next few months with higher precipitation. As precipitation events begins, the ratio of estimated baseflow to streamflow begins to decrease. During rainfall periods, the ratio of estimated baseflow to streamflow decreases from 0.90 ~ 1.00 to 0.20 ~ 0.60, and the monthly average ratio also becomes lower when precipitation is high during that month, such as the monthly average ratio of 0.55 in October. The yearly average ratio of estimated baseflow to streamflow is 0.78 from 2013 to 2014. Moreover, the ratio of estimated

baseflow to streamflow also changes in different seasons. During the winter season, which is from November to April, the monthly average ratios of estimated baseflow to streamflow are approximately from 0.70 ~ 0.90, whereas in other seasons, from May to October, the monthly average ratios are approximately from 0.60 ~ 0.80 (Figure 11). The ratios of estimated baseflow to streamflow in winter are generally higher than the ratio during other seasons.

In terms of synthetic baseflow, the values of baseflow obtained from HGS is generally lower than baseflow obtained from the various estimation approaches, thus the ratio of synthetic baseflow to streamflow is always lower than the ratio of estimated baseflow to streamflow. The daily ratio of synthetic baseflow to streamflow, the monthly average ratio, and the yearly average ratio are all lower than equivalent ratios computed with estimated baseflow. Moreover, the overall change of the ratio computed with synthetic baseflow shows similar features when compared to the ratio based on estimated baseflow. During dry seasons, the ratio of synthetic baseflow to streamflow is approximately 0.70 ~ 1.00, higher than that of the rainy season, ranging approximately between 0.30 ~ 0.60. For example, the monthly average ratio for August 2013 is 0.74, which is higher than the monthly average 0.46 in June and the monthly average ratio of 0.42 for October 2013 with higher precipitation. In different seasons, the ratio of synthetic baseflow to streamflow is also generally higher in winter and lower in other seasons, as is the case with estimated ratio. During the winter season, which is from November to April, monthly average ratios of estimated baseflow to streamflow are approximately from 0.60 ~ 0.70, whereas in other seasons, from May to October, the monthly average ratios are approximately from 0.40 ~ 0.60 (Figure 11).

Chapter 6

Discussion

6.1 Comparison of baseflow estimation techniques with real data

From the estimated baseflow calculated based on real streamflow data (Figure 5), it is observed that the baseflow hydrographs estimated through different approaches show different features. For the graphical approaches (Figures 5a-d), as mentioned previously, linear interpolation is utilized, leading to dramatically large increases of baseflow during precipitation events. In addition, the use of relative minimum streamflow values representing baseflow over certain time intervals results in staircase patterns, which are abnormal features that are not observed under natural conditions.

For the digital filter approaches (Figures 5e-j), different filters and their determination of the most optimal parameters are dependent on environmental conditions of the watershed of interest. Figure 5 shows that the baseflow hydrographs obtained through filter approaches are generally smoother than their graphical counterparts.

As for the Lyne and Hollick (Figure 5e), Eckhardt (Figure 5h), as well as Furey and Gupta (Figure 5i) approaches, baseflow significantly increases during precipitation events, especially for the Furey and Gupta approach. For the Lyne and Hollick approach, the portion of baseflow relative to total streamflow is smaller than that in the Furey and Gupta approach, which could be as high as 35%. The baseflow percent of the Eckhardt approach is also around 35%, whereas the baseflow hydrograph of the Eckhardt approach is smoother. Figure 5i shows that baseflow could even take up to 50% of streamflow during rainfall

periods when using the Furey and Gupta approach, and the response of baseflow to precipitation events is rapid, which is not consistent with the slow-response features of baseflow. For the Chapman and Maxwell (Figure 5f) as well as the EWMA (Figure 5j) approaches, there is no large increase during precipitation, and baseflow accounts for approximately 15% of streamflow. The baseflow hydrograph obtained through the Chapman and Maxwell approach is smoother than the EWMA approach.

In general, the baseflow hydrograph obtained with the FUKIH approach (Figure 5g) is the flattest and smoothest. This is due to the fact that the FUKIH approach initially involves the UKIH approach, while a filter is then applied during the second stage, resulting in a baseflow hydrograph that does not show any sudden increases during precipitation events and is relatively flat over the three-year time period over which the analysis is conducted.

However, although some abnormal features could be observed from the analysis of these hydrographs obtained through different baseflow estimation techniques, it is hard to directly determine which one is the most optimal estimation technique based on hydrologic plausibility. In order to assess the performance of each technique and to determine the optimal one, true baseflow values are needed. Due to the lack of true baseflow measurements at the ACW, synthetic data generated with HGS were utilized to in this study to further assess the different baseflow estimation techniques.

6.2 Comparison of baseflow estimation techniques with synthetic data

In this study, HGS is utilized to generate synthetic streamflow and baseflow hydrographs at ten different monitoring points within the ACW. The synthetic baseflow hydrograph outputted from HGS is considered to be the true baseflow hydrograph and

compared with estimated baseflow hydrographs computed using the ten baseflow estimation techniques from the synthetic streamflow hydrograph. While the HGS-generated baseflow hydrograph is considered as true baseflow, one needs to acknowledge that sophisticated numerical models could still produce errors during simulations. This is so even if all known salient hydrological processes and large amounts of data are incorporated into the model to accurately simulate the conditions of the ACW. For example, in this model, baseflow at one point is simulated by adding up the exchange fluxes at all the nodes from upstream to that point, thus the resolution of the model grid could potentially impact simulation results. Therefore, even if high-resolution models are utilized, one cannot ensure that simulated streamflow and baseflow hydrographs are free of numerical errors. Also, the soil and underlying layers as well as land use in this model are divided into several categories, but the distribution and division of different types of soil, geological units, as well as land use, are far more intricate in the actual watershed. All of these abovementioned factors could impact simulation results, leading to potential errors in synthetic streamflow and baseflow that are computed with HGS.

Figure 8 shows that synthetic baseflow is flat and smooth throughout the entire three-year period. The values of synthetic baseflow are relatively low and do not dramatically increase during rainfall. Compared with the synthetic baseflow hydrograph, the estimated baseflow hydrograph calculated through the Furey and Gupta approach (Figure 8i) shows large values that are several times larger than synthetic baseflow. The baseflow hydrographs estimated through the Eckhardt (Figure 8h) as well as Lyne and Hollick (Figure 8e) approaches are also considerably higher than the synthetic baseflow hydrograph. As for the three graphical approaches, when compared to the smooth synthetic

baseflow hydrograph, the estimated baseflow contains numerous shark peaks and staircase patterns that are not hydrologically plausible. Among all ten baseflow estimation approaches, the FUKIH approach (Figure 8g) generates baseflow that is most similar to synthetic baseflow, both in terms of their magnitude and features of the baseflow hydrographs.

In order to quantitatively assess which baseflow estimation technique yields values that are closest to synthetic baseflow estimated with HGS, model performance metrics such as the *NSE* number, as well as L_1 and L_2 norms are utilized. Results reveal that the most optimal baseflow estimation approach varies from point to point for the ACW.

According to previous research on baseflow estimation techniques (Partington et al., 2012), baseflow behavior at different locations might be different due to variations in environmental factors such as land use, topography, geology, slope, and hydraulic parameters to name a few, and different baseflow estimation approaches result in baseflow hydrographs with different behavior and features. For example, the baseflow hydrograph estimated through the FUKIH approach is always relatively lower than other approaches and baseflow values do not significantly increase during precipitation events due to the second filtration by the digital approach, thus this approach may be most suitable for catchments where the baseflow values are low and do not have dramatic variations. Other baseflow separation techniques examined in this study may be more suitable under different environmental conditions. In order to better understand the influence of various environmental factors on baseflow, additional research is needed. The improved understanding of baseflow genesis mechanisms should lead to improved management of watersheds.

Chapter 7

Summary and conclusions

Baseflow is a vital water cycle component to understand watershed hydrology and surface water/groundwater interaction. In this study, baseflow is studied and estimated at the ACW from May 2013 to December 2016 through several baseflow estimation techniques, including four graphical and six digital filter approaches, to analyze features of baseflow and to evaluate the performances of each approach.

After estimating baseflow at a gauging station obtained through all these approaches and analyzing the results, it has been concluded that it is hard to determine the most optimal baseflow estimation approach based on the concept of hydrologic plausibility (Nathan and McMahon, 1990) alone. This is because the concept of hydrologic plausibility is always subjective. Therefore, reliable baseflow estimates along river reaches and their variations with seasons are needed to assess the performance of each baseflow estimation technique, although such records are not readily available.

In previous studies, some researchers used fully integrated three-dimensional models to simulate baseflow values (e.g., Partington et al., 2012; Li et al., 2014; Su et al., 2016). However, the 3D integrated hydrologic model used in previous studies to conduct the analysis was based on monotonically sloping V-shaped catchments, which simplifies the actual intricate conditions in a natural environment. In this study, a high resolution HGS model of the ACW is constructed and run by Tong et al. (2022) to simulate both surface water and baseflow hydrographs from 2013 to 2016. The simulated baseflow hydrograph from HGS is treated as the actual baseflow and utilized to investigate the performances of ten baseflow estimation approaches.

Our study resulted in the following conclusions:

1. From the baseflow hydrograph estimated with actual streamflow data at a gauging station, it could be inferred that the baseflow hydrographs obtained through graphical approaches always show abnormal patterns caused by the linear interpolation used in graphical approaches, such as staircase patterns and shark peaks. These features reflect sudden changes to estimated baseflow, which is not in accordance with natural conditions. Also, in graphical approaches, baseflow hydrographs always show a large increase during significant precipitation events of longer durations. This phenomenon has also been observed in the Furey and Gupta approach, which is not hydrologically plausible.
2. From the values of time derivations (dQ/dt) computed from baseflow hydrograph, it is observed that in graphical approaches, the dQ/dt of baseflow is dramatically large during rainfall for the HYSEP fixed- and sliding-interval approaches, and the dQ/dt of baseflow is even nearly the same as streamflow during the beginning of some precipitation events. This is not consistent with the anticipated delayed response of baseflow, and this high increasing rate of baseflow is also not hydrologically plausible. These large dQ/dt values are also observed when the Furey and Gupta approach is applied to the hydrographs. Based on the abnormal dQ/dt values, these three baseflow estimation approaches are not considered to be good estimation approaches. Together with the examination of baseflow hydrograph, the use of dQ/dt has been found to be very useful in assessing the hydrologic plausibility of baseflow estimation techniques.
3. As true baseflow hydrographs are not available at the ACW, synthetic baseflow hydrographs generated with the HGS model at ten study points situated at various

locations within the watershed are utilized as true baseflow to help assess the performances of baseflow estimation techniques. Examination of synthetic baseflow at ten study points revealed that they are, in general, flat and smooth throughout the year. It does not show any significant increases between or during precipitation events, and generally the baseflow values are low, which is only around 5% to 10% of streamflow during the precipitation. Compared with synthetic results, the estimated baseflow hydrographs obtained through the Eckhardt, Lyne and Hollick, as well as Furey and Gupta approaches are several times higher than synthetic baseflow during rainy seasons, and this was especially the case for the Furey and Gupta approach. The estimated baseflow hydrographs using the FUKIH approach is most similar to results from HGS, and they both exhibit low baseflow values and flat baseflow hydrographs for the ACW.

4. To quantitatively evaluate the goodness of fit of baseflow values computed from each baseflow estimation approach with synthetic baseflow from HGS, model performance metrics are utilized. From the scatterplots and regression lines, it is inferred that synthetic baseflow is relatively low, thus it is generally smaller than estimated baseflow in most cases. In particular, the *NSE* number, as well as L_1 and L_2 norms, are also calculated for ten baseflow estimation approaches at ten different monitoring locations within the ACW, and the results show that the most optimal approaches at different locations are not constant from point to point. Of the ten monitoring points, the FUKIH approach ranked the best at six points. The Chapman and Maxwell approach ranked to have the best performance at three points and the Eckhardt approach yielded the best results at one point.

5. From the baseflow hydrographs at ten study points, the seasonal patterns of the change of baseflow could be obviously observed. During summertime, baseflow becomes slightly higher corresponding to higher precipitation, whereas during wintertime, baseflow always decreases. After comparing baseflow and streamflow hydrographs, the increasing amount and rate of baseflow are much smaller than the streamflow when there is a precipitation event, corresponding with the feature of baseflow—it always shows a delayed response to precipitation events. During rainy days, the ratio of baseflow to streamflow varies from 0.2 to 0.6, whereas during dry seasons, virtually all of streamflow constitutes baseflow underscoring the importance of groundwater to watershed fluxes. The ratio of baseflow to streamflow also varies in different seasons. During winter season, from November to April, the ratio of baseflow to streamflow is generally higher than the ratio during other seasons from May to October.
6. At different study locations within the ACW, the most optimal baseflow estimation technique is not the same. In particular, baseflow hydrographs at different location might be different caused through spatiotemporal variations in hydrological and geologic conditions. Therefore, the baseflow estimation technique that generates reasonable baseflow estimates may vary with environmental factors such as land use, topography, geology, slope, and hydraulic parameters to name a few. Further studies on how spatiotemporal variability in hydrological and geological conditions affect baseflow need to be investigated to better understand the factors that influence the genesis of baseflow and to also help the investigation of the selection of baseflow estimation technique in a more rigorous fashion.

References

Aksoy, H., Kurt, I., & Eris, E. (2009). Filtered smoothed minima baseflow separation method. *Journal of Hydrology*, *372*(1-4), 94-101.

Aksoy, H., Unal, N. E., & Pektas, A. O. (2008). Smoothed minima baseflow separation tool for perennial and intermittent streams. *Hydrological Processes: An International Journal*, *22*(22), 4467-4476.

Arnold, J. G., & Allen, P. M. (1999). Automated methods for estimating baseflow and ground water recharge from streamflow records 1. *JAWRA Journal of the American Water Resources Association*, 35(2), 411-424.

Arnold, J. G., Muttiah, R. S., Srinivasan, R., & Allen, P. M. (2000). Regional estimation of base flow and groundwater recharge in the Upper Mississippi river basin. *Journal of Hydrology*, *227*(1-4), 21-40.

Aquanty Inc (2018). HydroGeoSphere. A three-dimensional numerical model describing fully-integrated subsurface and surface flow and solute transport. Retrieved from Waterloo, Ontario, Canada. https://www.aquanty.com/hgs-download.

Brodie, R., Sundaram, B., Tottenham, R., Hostetler, S., & Ransley, T. (2007). An overview of tools for assessing groundwater-surface water connectivity. *Bureau of Rural Sciences, Canberra, Australia*, *131*.

Cey, E. E., Rudolph, D. L., Parkin, G. W., Aravena, R. (1998). Quantifying groundwater discharge to a small perennial stream in southern Ontario, Canada, *J. Hydrol*., 210, 21-37.

Chapman, T. G. (1991). Comment on "Evaluation of automated techniques for base flow and recession analyses" by RJ Nathan and TA McMahon. *Water Resources Research*, *27*(7), 1783-1784.

Chapman, T. G. (1999). A comparison of algorithms for stream flow recession and baseflow separation. *Hydrological Processes*, *13*(5), 701-714.

Chapman, T. G., & Maxwell, A. I. (1996). Baseflow separation-comparison of numerical methods with tracer experiments. In *Hydrology and Water Resources Symposium 1996: Water and the Environment; Preprints of Papers* (p. 539). Institution of Engineers, Australia.

Chow, R., Frind, M. E., Frind, E. O., Jones, J. P., Sousa, M. R., Rudolph, D. L., Molson, J. W., & Nowak, W. (2016). Delineating baseflow contribution areas for streams–A model and methods comparison. *Journal of Contaminant Hydrology*, *195*, 11-22.

Conant, B. (2004). Delineating and quantifying ground water discharge zones using streambed temperatures, *Ground water,* 42(2) 243-257.

Eckhardt, K. (2005). How to construct recursive digital filters for baseflow separation. *Hydrological Processes: An International Journal*, 19(2), 507-515.

Environment and Natural Resources—Historical Hydrometric Data. (2019). Retrieved from https://wateroffice.ec.gc.ca/search/historical_e.html

Furey, P. R., & Gupta, V. K. (2001). A physically based filter for separating base flow from streamflow time series. *Water Resources Research*, *37*(11), 2709-2722.

Gonzales, A. L., Nonner, J., Heijkers, J., & Uhlenbrook, S. (2009). Comparison of different base flow separation methods in a lowland catchment. *Hydrology and Earth System Sciences*, *13*(11), 2055-2068.

Grand River Conservation Authority. (2001). *Alder Creek Watershed Study. Phase 1-Disscusion Paper.* Draft report prepared for the Regional Municipality of Waterloo.

Grand River Conservation Authority. (2009). Integrated Water Budget Report, Grand River Watershed. Retrieved from https://www.grandriver.ca/en/our-watershed/resources/Documents/Water_Supplies_WaterBudget_2009.pdf

Grand River Conservation Authority. (2018). Geology of the Grand River Watershed. Retrieved from https://www.grandriver.ca/en/our-watershed/resources/Documents/Groundwater/Watershed-Geology_March272019.pdf

Grand River Conservation Authority. (2019). *Maps and data*. Retrieved from https://www.grandriver.ca/en/our-watershed/Maps-and-data.aspx

Government of Canada. (2019). *Surficial geology*. Retrieved from https://www.geologyontario.mndm.gov.on.ca/ogsearth.html#surficial-geology

Government of Canada. (2020). Past Weather and Climate, Historical Data for Roseville Weather Station. Retrieved from https://climate.weather.gc.ca/historical_data/search_historic_data_e.html

Hall, F. R. (1968). Base-flow recessions—A review. *Water Resources Research*, *4*(5), 973-983.

Holysh, S., J. Pitcher, and D. Boyd. (2001). Grand River Regional Groundwater Study. *Grand River Conservation Authority*.

Hooper, R. P., & Shoemaker, C. A. (1986). A comparison of chemical and isotopic hydrograph separation. *Water Resources Research*, *22*(10), 1444-1454.

Indarto, I., Novita, E., & Wahyuningsih, S. (2016). Preliminary study on baseflow separation at watersheds in East Java regions. *Agriculture and Agricultural Science Procedia, 9*, 538 – 550.

Institute of Hydrology. (1980). Low Flow Studies. Research Report, Wallingford, Oxon.

Kalbus, E., Reinstorf, F., & Schirmer M. (2006). Measuring methods for groundwater – surface water interactions: a review, *Hydrology and Earth System Sciences*, *10*(6), 873–887.

Kaviany E. (1978). Zur Hydrogeologie im Niederschlagsgebiet der Dill (Hessen). *Gießener Geologische Schriften* 19: 248.

Lim, K. J., Engel, B. A., Tang, Z., Choi, J., Kim, K. S., Muthukrishnan, S., & Tripathy, D. (2005). Automated web GIS based hydrograph analysis tool, WHAT 1. *JAWRA Journal of the American Water Resources Association*, *41*(6), 1407-1416.

Lott, D. A., & Stewart, M. T. (2013). A power function method for estimating base flow. *Groundwater*, *51*(3), 442-451.

Lott, D. A., & Stewart, M. T. (2016). Base flow separation: A comparison of analytical and mass balance methods. *Journal of Hydrology*, 535, 525-533.

Lyne, V., & Hollick, M. (1979). Stochastic time-variable rainfall-runoff modelling. In *Institute of Engineers Australia National Conference* (Vol. 1979, pp. 89-93). Barton, Australia: Institute of Engineers Australia.

Matrix Solutions Inc., S.S. Papadopulos and Associates (2014a). Region of Waterloo Tier Three Water Budget and Local Area Risk Assessment; Model Calibration and Water Budget Report. August, 2014.

Matrix Solutions Inc., S.S. Papadopulos and Associates (2014b). Region of Waterloo Tier Three Water Budget and Local Area Risk Assessment; Final Risk Assessment Report. September, 2014.

Miller, M. P., Buto, S. G., Susong, D. D., & Rumsey, C. A. (2016). The importance of base flow in sustaining surface water flow in the Upper Colorado River Basin. *Water Resources Research*, 52(5), 3547-3562.

Nathan, R. J., & McMahon, T. A. (1990). Evaluation of automated techniques for base flow and recession analyses. *Water Resources Research*, *26*(7), 1465-1473.

Ontario Ministry of Natural Resources. (2008). Southern Ontario Land Resource Information System (SOLRIS) Land Use Data [computer file]. Toronto, ON. Accessed 20 Jan 2014.

Rosenberry, D.O., LaBaugh, J.W. (2008), *Field techniques for estimating water fluxes between surface water and ground water*. United States Geological Survey Techniques and Methods 4–D2, 128 pgs.

Rutledge, A. T. (1998). Computer programs for describing the recession of ground-water discharge and for estimating mean ground-water recharge and discharge from

streamflow records: Update (No. 98). US Department of the Interior, US Geological Survey.

Schwartz, S. S. (2007). Automated Algorithms for Heuristic Base-Flow Separation 1. *JAWRA Journal of the American Water Resources Association*, *43*(6), 1583-1594.

Sklash, M. G., & Farvolden, R. N. (1979). The role of groundwater in storm runoff. *Journal of Hydrology, 43*(1-4), 45-65.

Sloto, R. A., & Crouse, M. Y. (1996). HYSEP: A computer program for streamflow hydrograph separation and analysis. *Water Resources Investigations Report*, *96*, 4040.

Spongberg, M. E. (2000). Spectral analysis of base flow separation with digital filters. *Water Resources Research*, *36*(3), 745-752.

Stewart, M., Cimino, J., & Ross, M. (2007). Calibration of base flow separation methods with streamflow conductivity. *Groundwater*, *45*(1), 17-27.

Su, C. H., Peterson, T. J., Costelloe, J. F., & Western, A. W. (2016). A synthetic study to evaluate the utility of hydrological signatures for calibrating a base flow separation filter. *Water Resources Research*, *52*(8), 6526-6540.

Tularam, G. A., & Ilahee, M. (2008). Exponential smoothing method of base flow separation and its impact on continuous loss estimates. *American Journal of Environmental Sciences*, *4*(2), 136.

Wahl, K. L., & Wahl, T. L. (1995). Determining the flow of comal springs at New Braunfels, Texas. *Proceedings of Texas Water*, *95*(6), 16-17.

Winter, T.C., Harvey, J.W., Franke, O.L., Alley, W.M. (1998), *Groundwater and Surface Water A Single Resource*, U.S. Geological Survey Circular 1139, Denver, Colorado, 87 pp.

Xie, J., Liu, X., Wang, K., Yang, T., Liang, K., & Liu, C. (2020). Evaluation of typical methods for baseflow separation in the contiguous United States. *Journal of Hydrology*, *583*, 124628.

Appendix

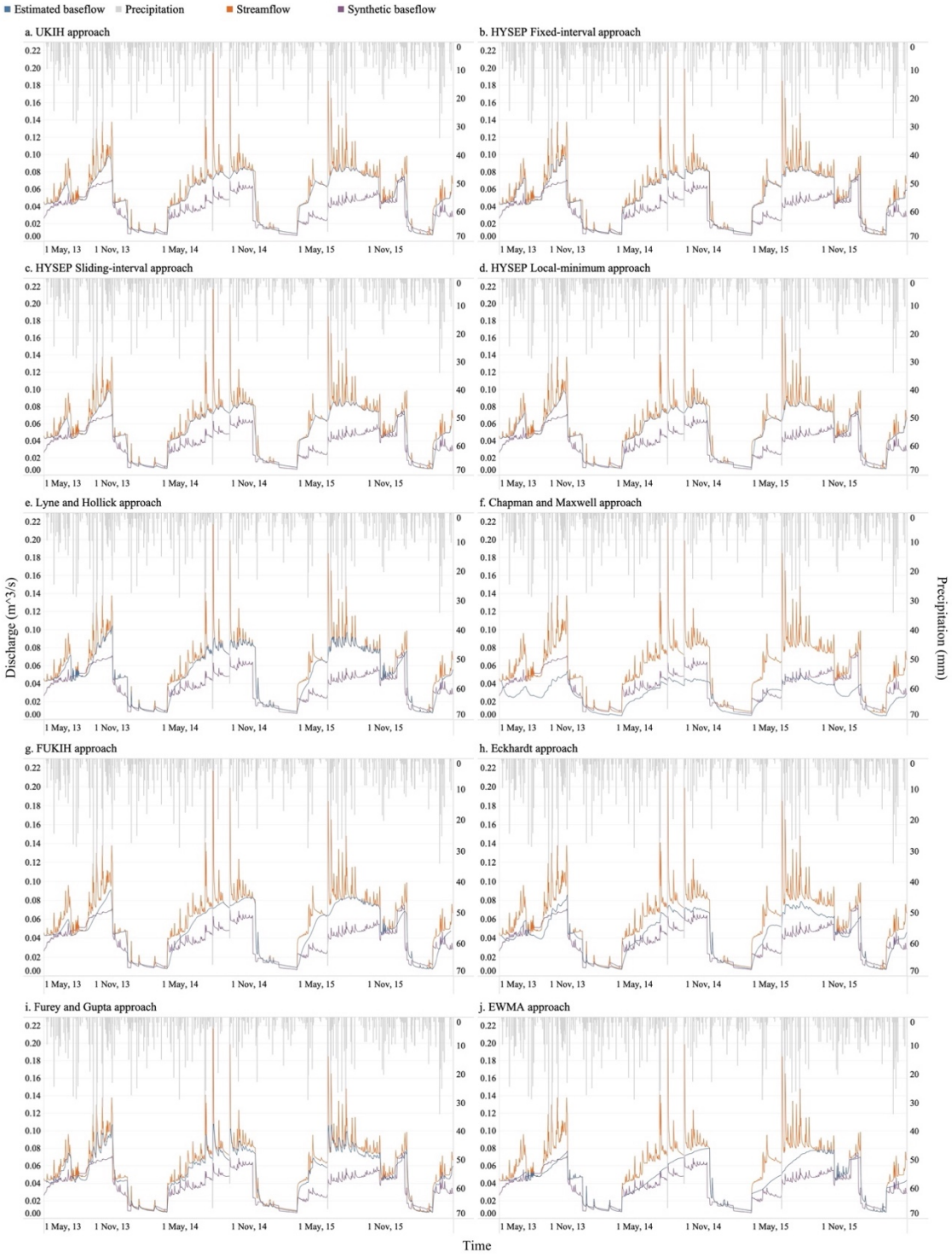

Figure A1. The comparison between synthetic baseflow obtained from the HGS model and estimated baseflow at Point 1 calculated through the: a) UKIH; b) HYSEP-Fixed interval; c) HYSEP-Sliding interval; d) HYSEP-Local minimum; e) Lyne and Hollick; f) Chapman and Maxwell; g) FUKIH; h) Eckhardt; i) Furey and Gupta; and j) EWMA approaches.

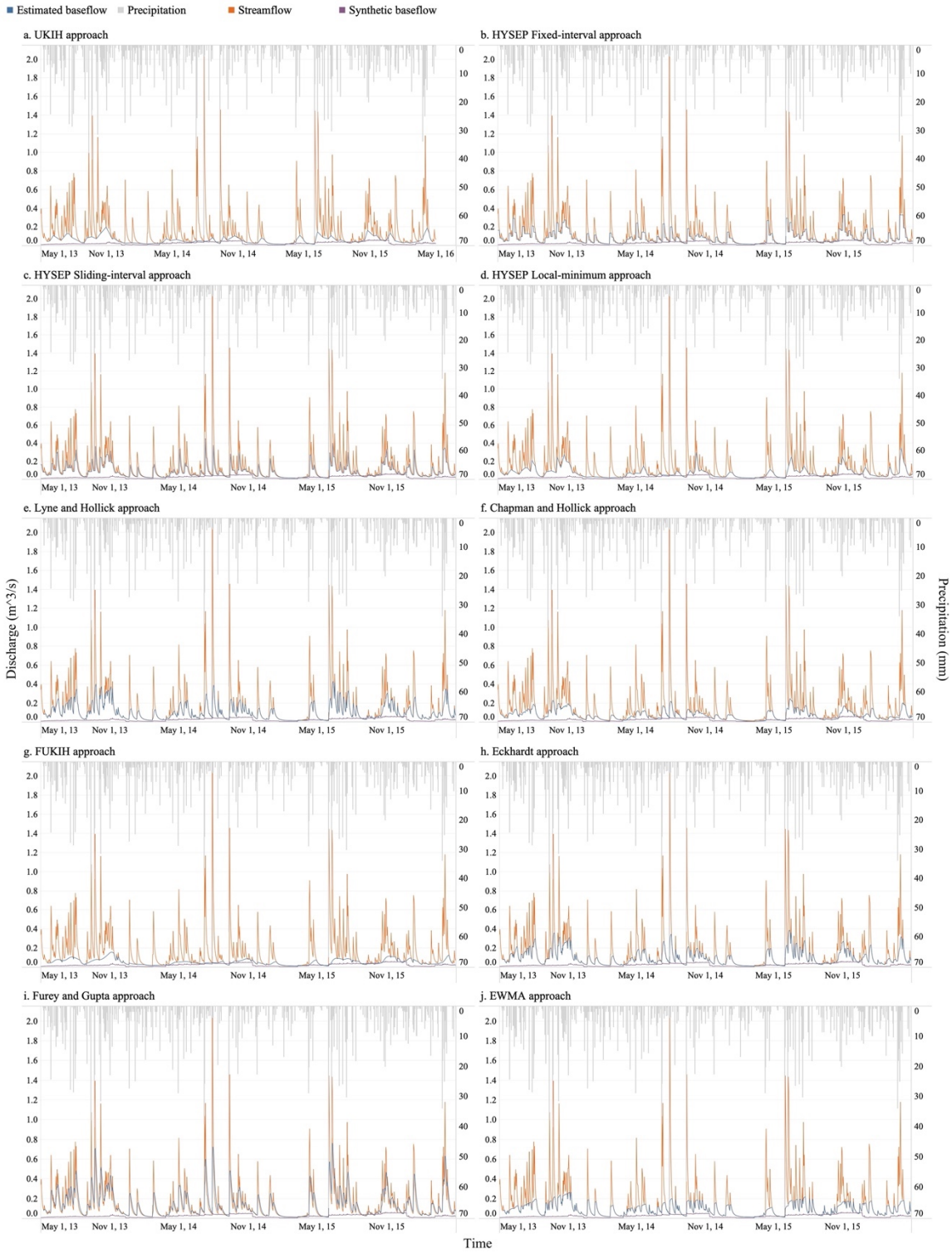

Figure A2. The comparison between synthetic baseflow obtained from the HGS model and estimated baseflow at Point 2 calculated through the: a) UKIH; b) HYSEP-Fixed interval; c) HYSEP-Sliding interval; d) HYSEP-Local minimum; e) Lyne and Hollick; f) Chapman and Maxwell; g) FUKIH; h) Eckhardt; i) Furey and Gupta; and j) EWMA approaches.

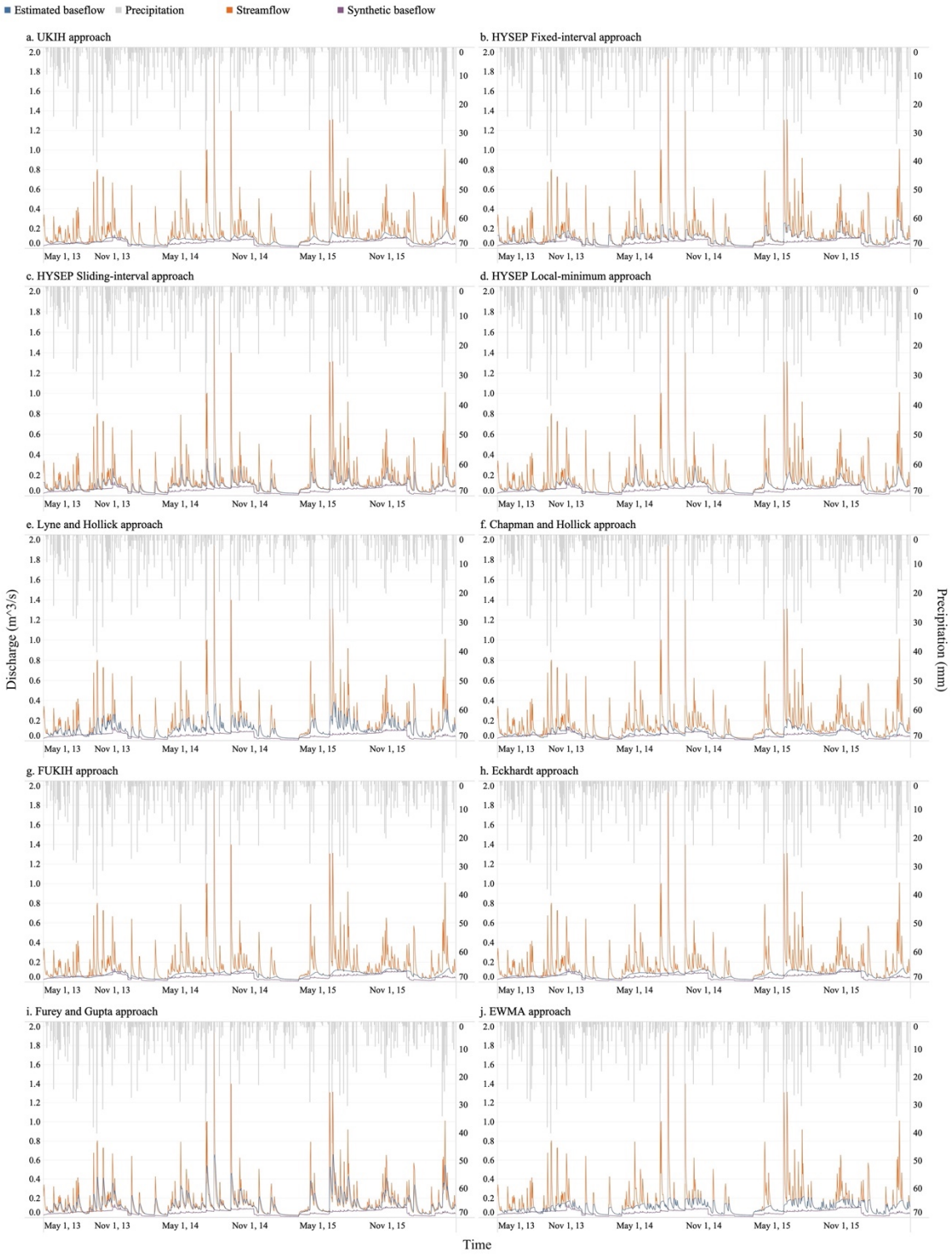

Figure A3. The comparison between synthetic baseflow obtained from the HGS model and estimated baseflow at Point 3 calculated through the: a) UKIH; b) HYSEP-Fixed interval; c) HYSEP-Sliding interval; d) HYSEP-Local minimum; e) Lyne and Hollick; f) Chapman and Maxwell; g) FUKIH; h) Eckhardt; i) Furey and Gupta; and j) EWMA approaches.

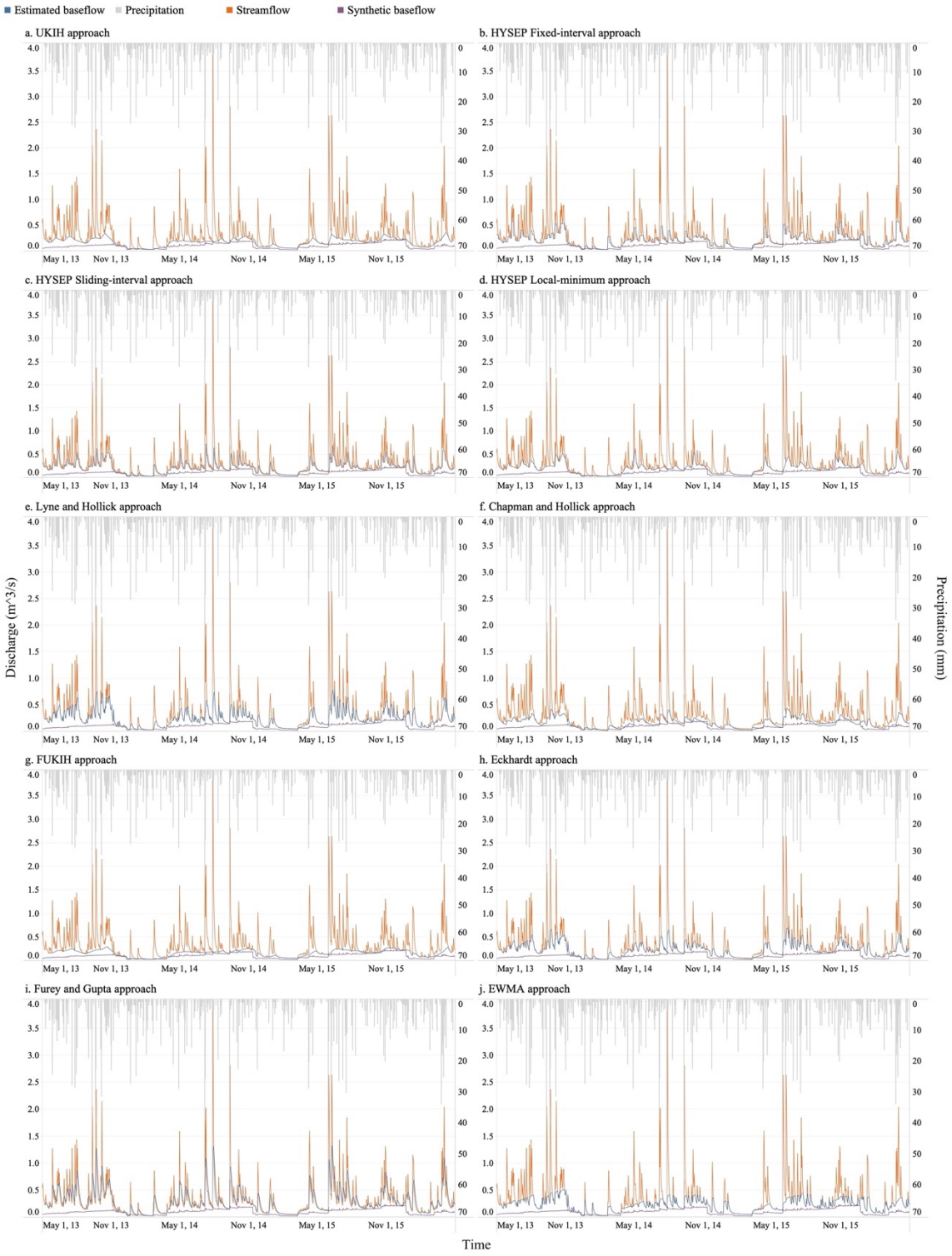

Figure A4. The comparison between synthetic baseflow obtained from the HGS model and estimated baseflow at Point 4 calculated through the: a) UKIH; b) HYSEP-Fixed interval; c) HYSEP-Sliding interval; d) HYSEP-Local minimum; e) Lyne and Hollick; f) Chapman and Maxwell; g) FUKIH; h) Eckhardt; i) Furey and Gupta; and j) EWMA approaches.

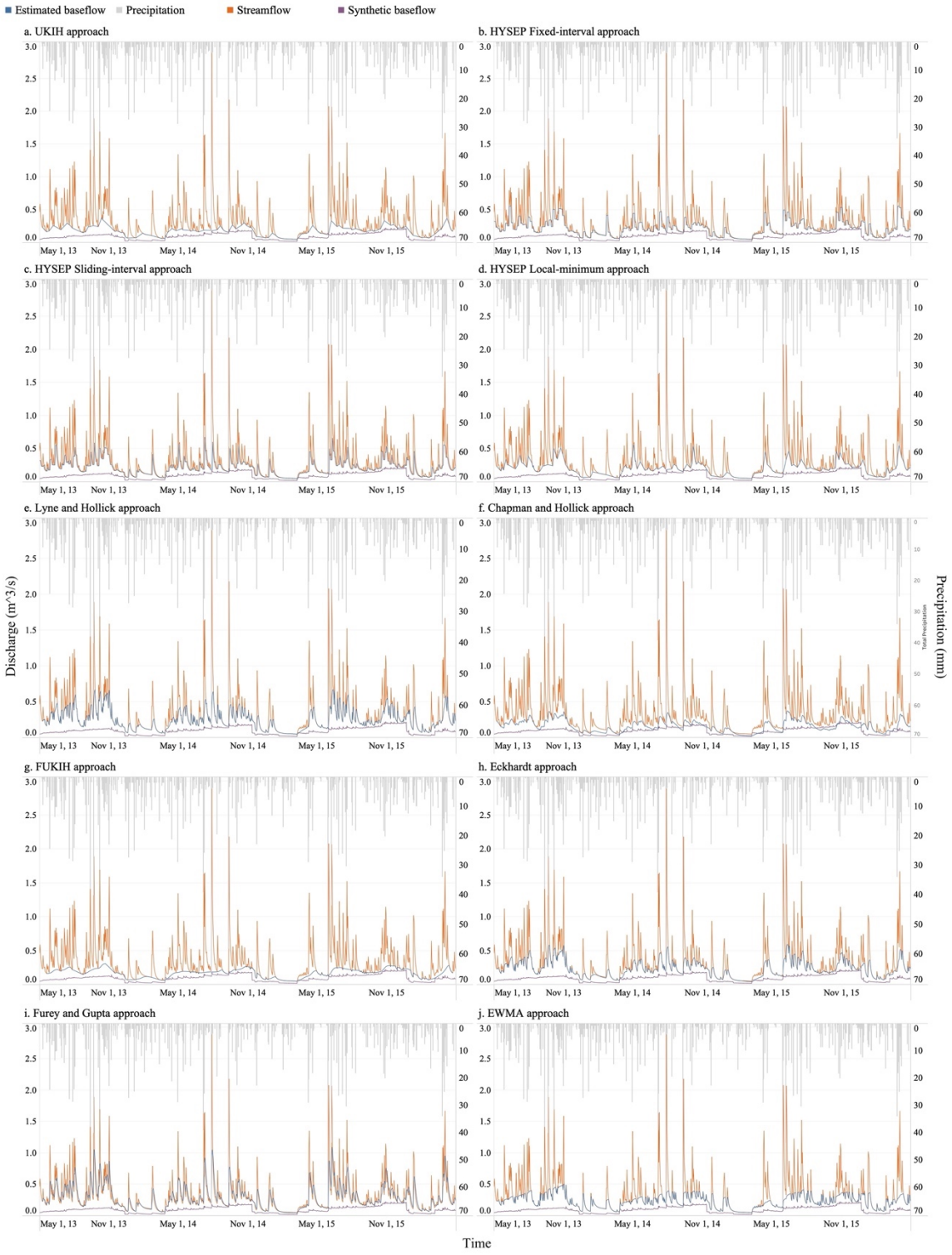

Figure A5. The comparison between synthetic baseflow obtained from the HGS model and estimated baseflow at Point 5 calculated through the: a) UKIH; b) HYSEP-Fixed interval; c) HYSEP-Sliding interval; d) HYSEP-Local minimum; e) Lyne and Hollick; f) Chapman and Maxwell; g) FUKIH; h) Eckhardt; i) Furey and Gupta; and j) EWMA approaches.

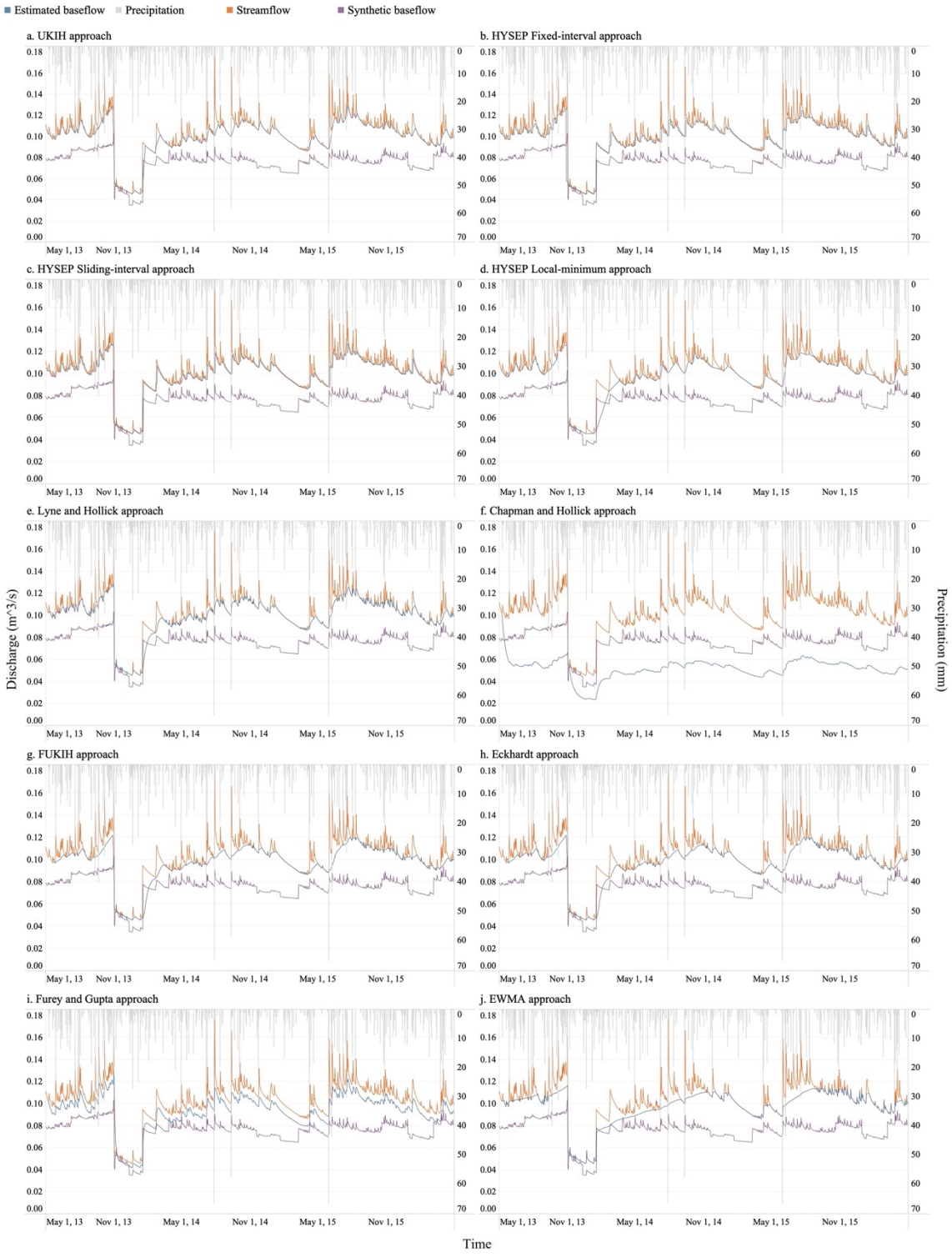

Figure A6. The comparison between synthetic baseflow obtained from the HGS model and estimated baseflow at Point 6 calculated through the: a) UKIH; b) HYSEP-Fixed interval; c) HYSEP-Sliding interval; d) HYSEP-Local minimum; e) Lyne and Hollick; f) Chapman and Maxwell; g) FUKIH; h) Eckhardt; i) Furey and Gupta; and j) EWMA approaches.

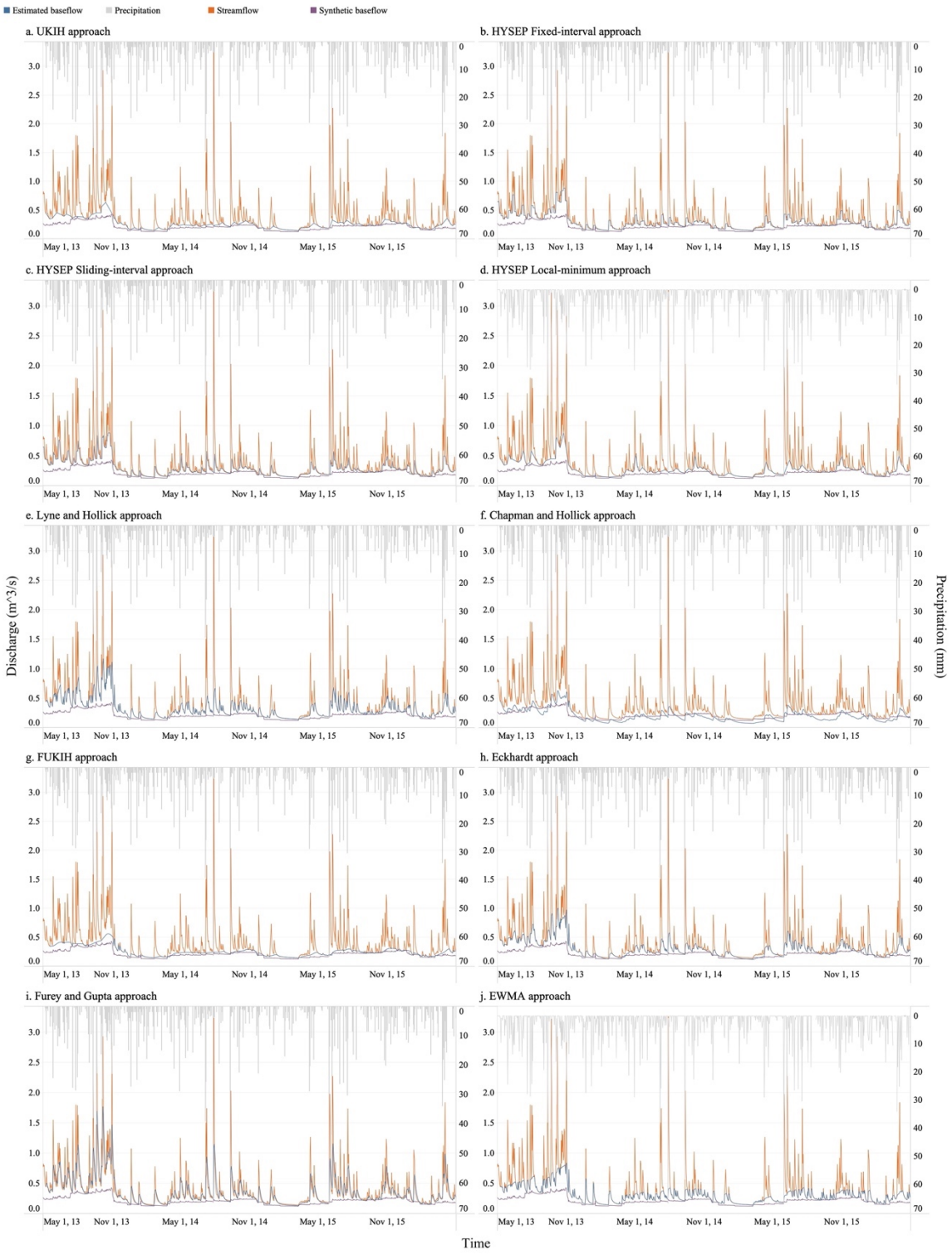

Figure A7. The comparison between synthetic baseflow obtained from the HGS model and estimated baseflow at Point 8 calculated through the: a) UKIH; b) HYSEP-Fixed interval; c) HYSEP-Sliding interval; d) HYSEP-Local minimum; e) Lyne and Hollick; f) Chapman and Maxwell; g) FUKIH; h) Eckhardt; i) Furey and Gupta; and j) EWMA approaches.

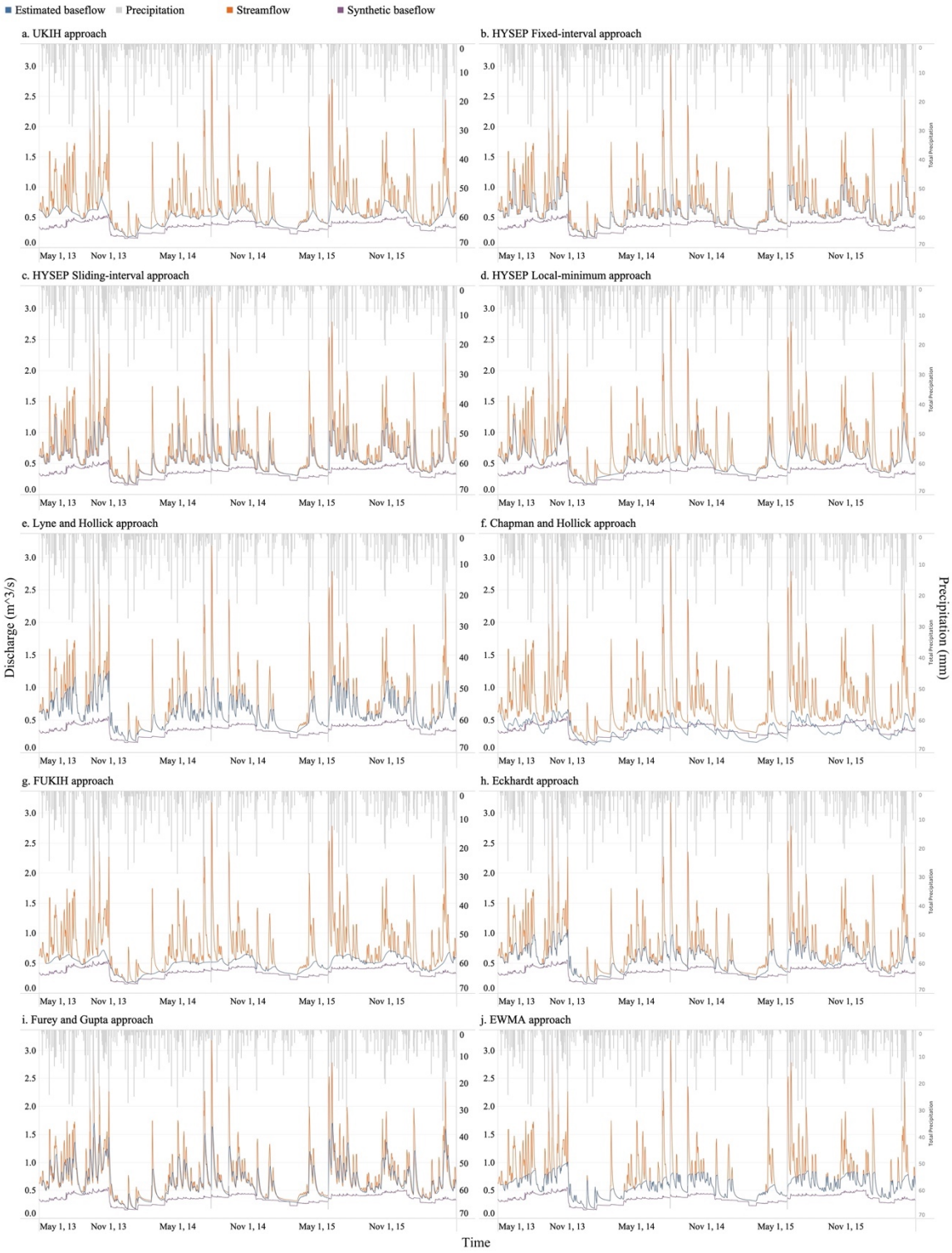

Figure A8. The comparison between synthetic baseflow obtained from the HGS model and estimated baseflow at Point 9 calculated through the: a) UKIH; b) HYSEP-Fixed interval; c) HYSEP-Sliding interval; d) HYSEP-Local minimum; e) Lyne and Hollick; f) Chapman and Maxwell; g) FUKIH; h) Eckhardt; i) Furey and Gupta; and j) EWMA approaches.

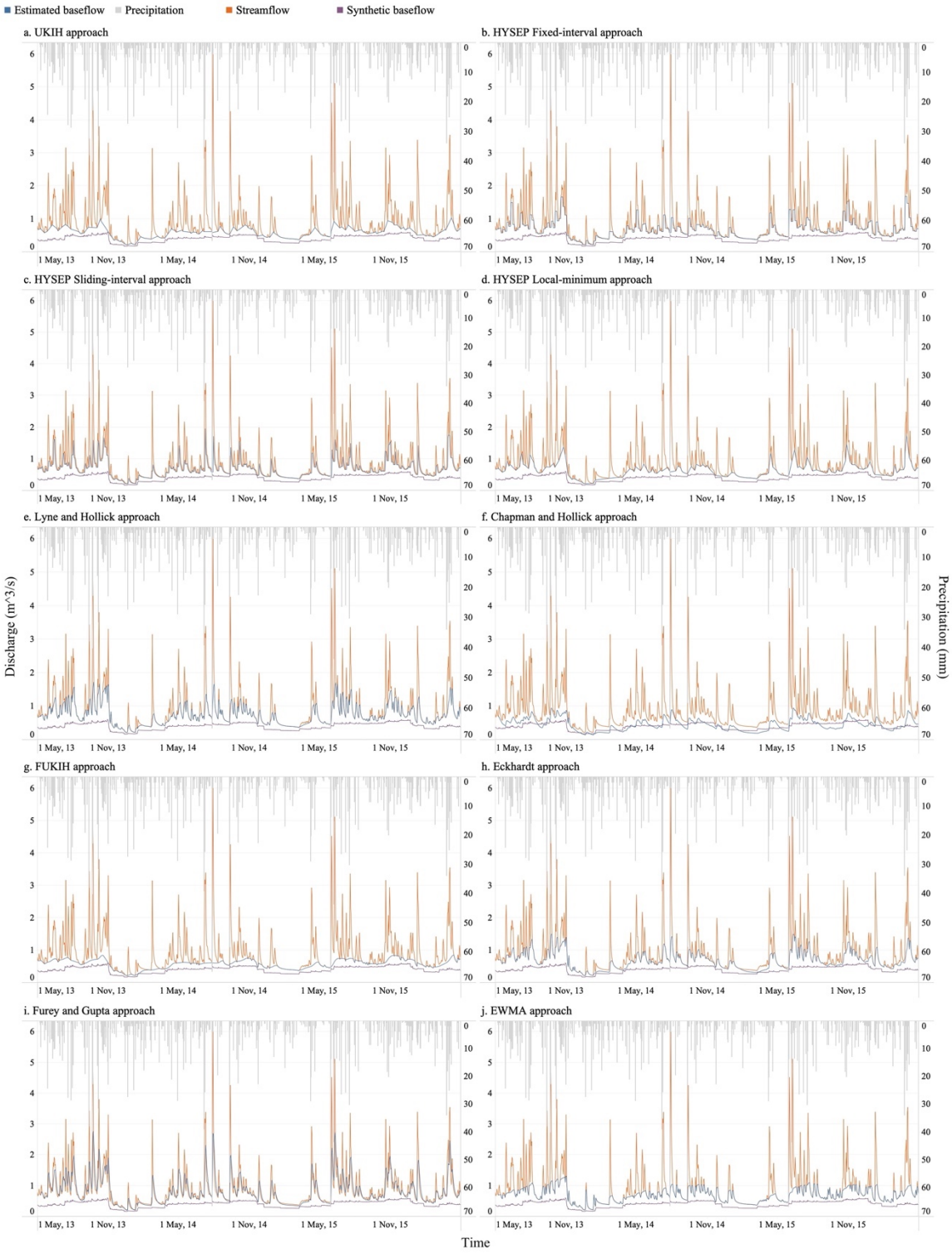

Figure A9. The comparison between synthetic baseflow obtained from the HGS model and estimated baseflow at Point 10 calculated through the: a) UKIH; b) HYSEP-Fixed interval; c) HYSEP-Sliding interval; d) HYSEP-Local minimum; e) Lyne and Hollick; f) Chapman and Maxwell; g) FUKIH; h) Eckhardt; i) Furey and Gupta; and j) EWMA approaches.

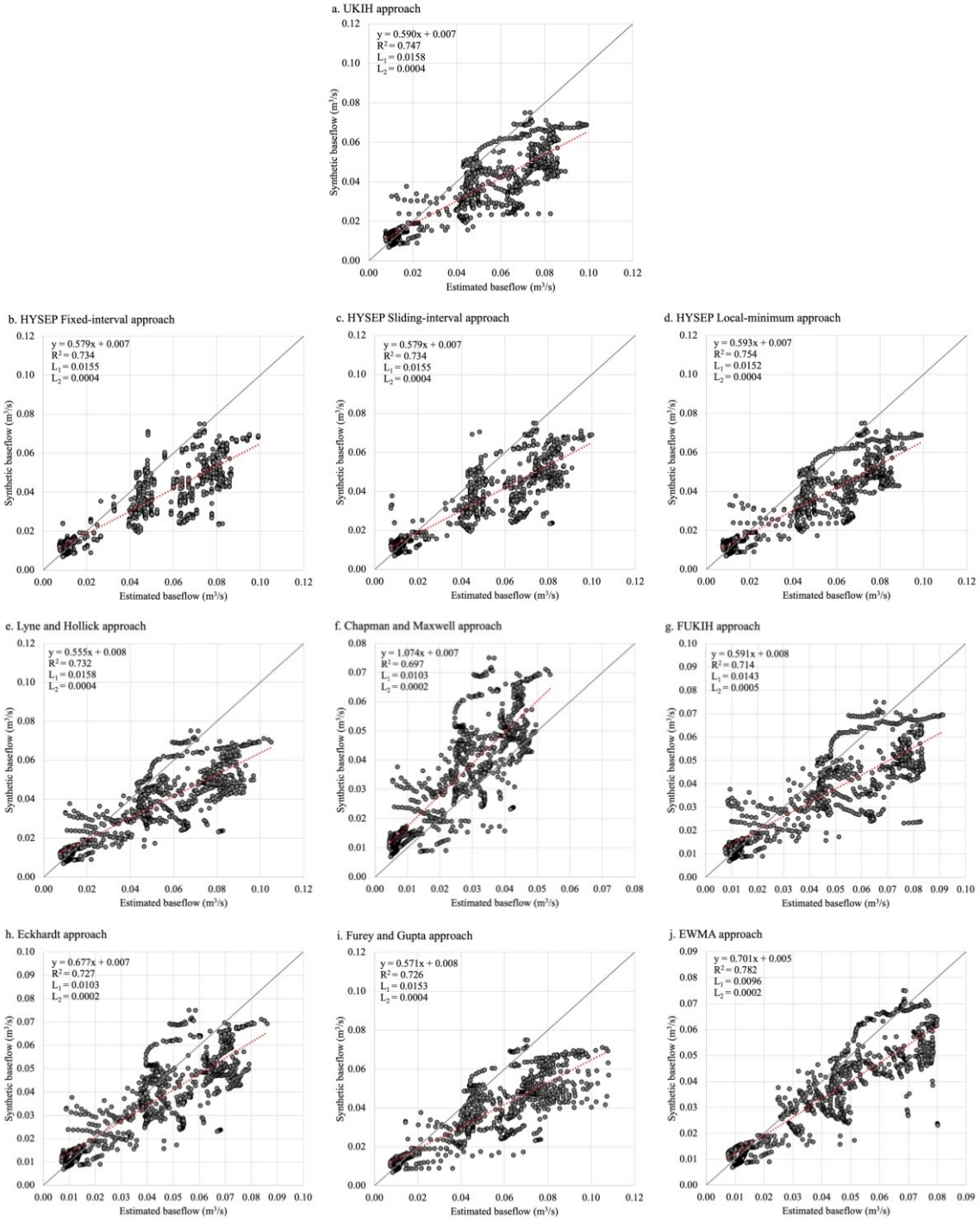

Figure A10. Scatter plots showing the relationship between synthetic baseflow obtained from the HGS model and estimated baseflow at Point 1 calculated through the: a) UKIH; b) HYSEP-Fixed interval; c) HYSEP-Sliding interval; d) HYSEP-Local minimum; e) Lyne and Hollick; f) Chapman and Maxwell; g) FUKIH; h) Eckhardt; i) Furey and Gupta; and j) EWMA approaches. The dashed red lines are the regression lines, while the solid black lines are the 1:1 lines describing a perfect fit.

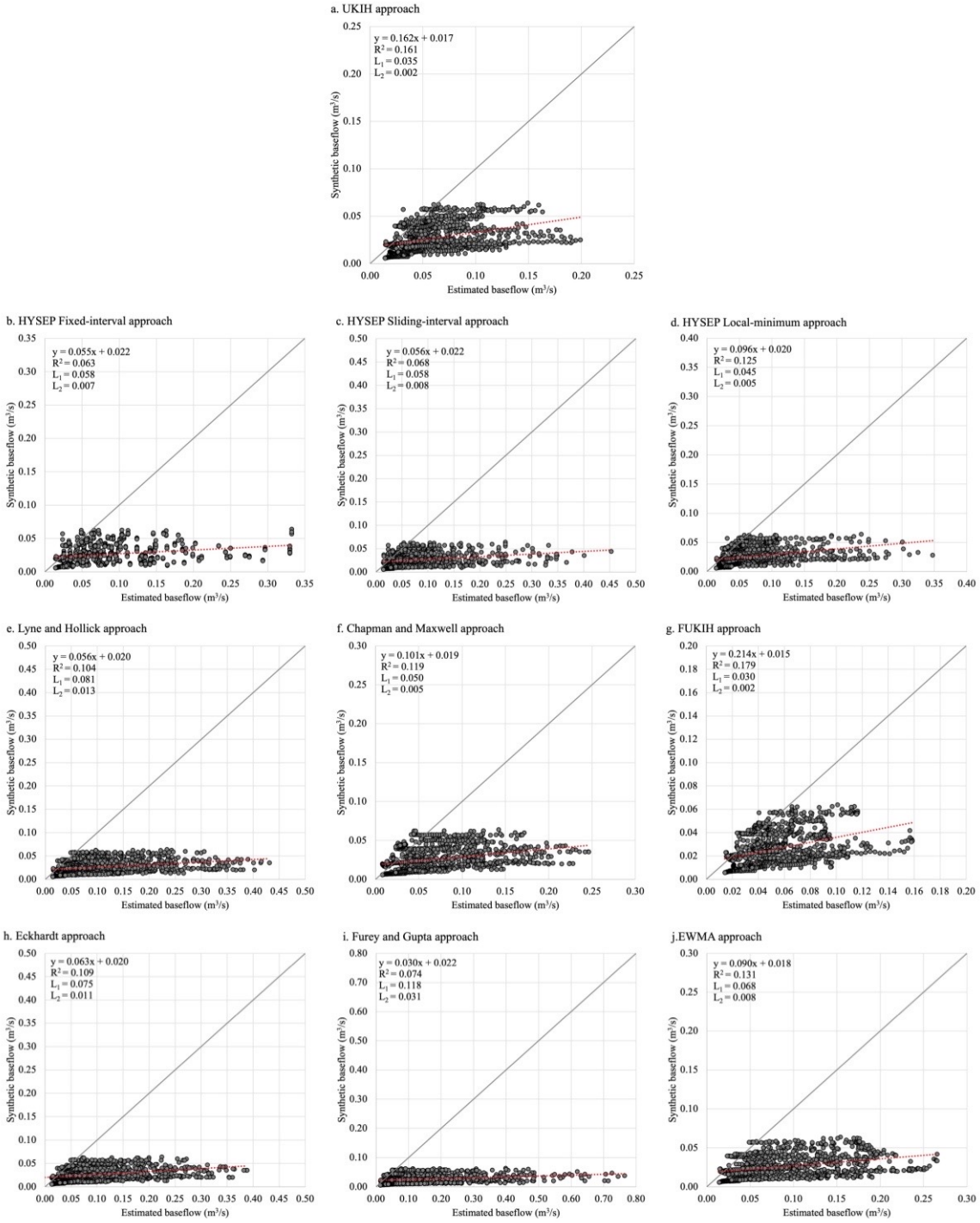

Figure A11. Scatter plots showing the relationship between synthetic baseflow obtained from the HGS model and estimated baseflow at Point 2 calculated through the: a) UKIH; b) HYSEP-Fixed interval; c) HYSEP-Sliding interval; d) HYSEP-Local minimum; e) Lyne and Hollick; f) Chapman and Maxwell; g) FUKIH; h) Eckhardt; i) Furey and Gupta; and j) EWMA approaches. The dashed red lines are the regression lines, while the solid black lines are the 1:1 lines describing a perfect fit.

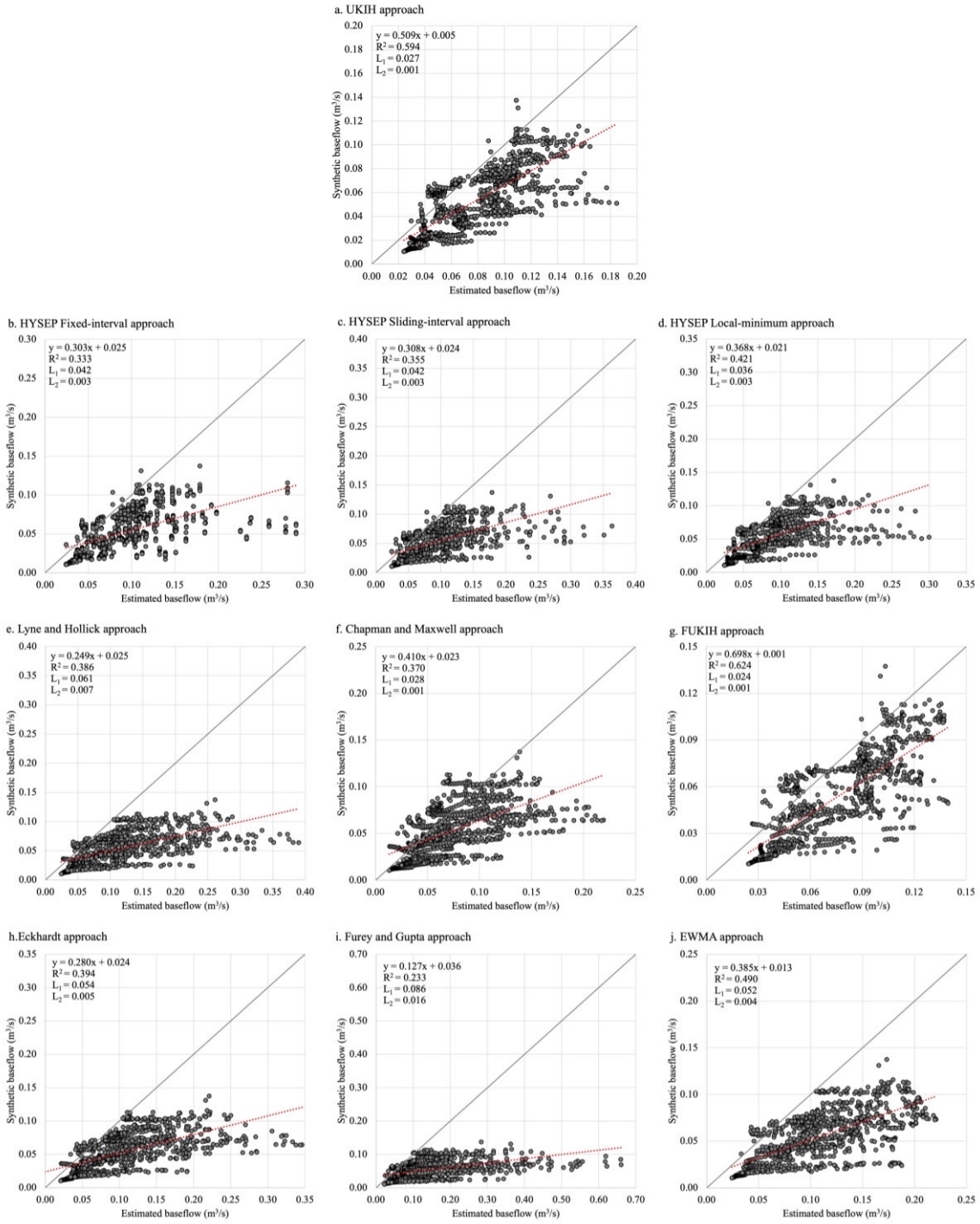

Figure A12. Scatter plots showing the relationship between synthetic baseflow obtained from the HGS model and estimated baseflow at Point 3 calculated through the: a) UKIH; b) HYSEP-Fixed interval; c) HYSEP-Sliding interval; d) HYSEP-Local minimum; e) Lyne and Hollick; f) Chapman and Maxwell; g) FUKIH; h) Eckhardt; i) Furey and Gupta; and j) EWMA approaches. The dashed red lines are the regression lines, while the solid black lines are the 1:1 lines describing a perfect fit.

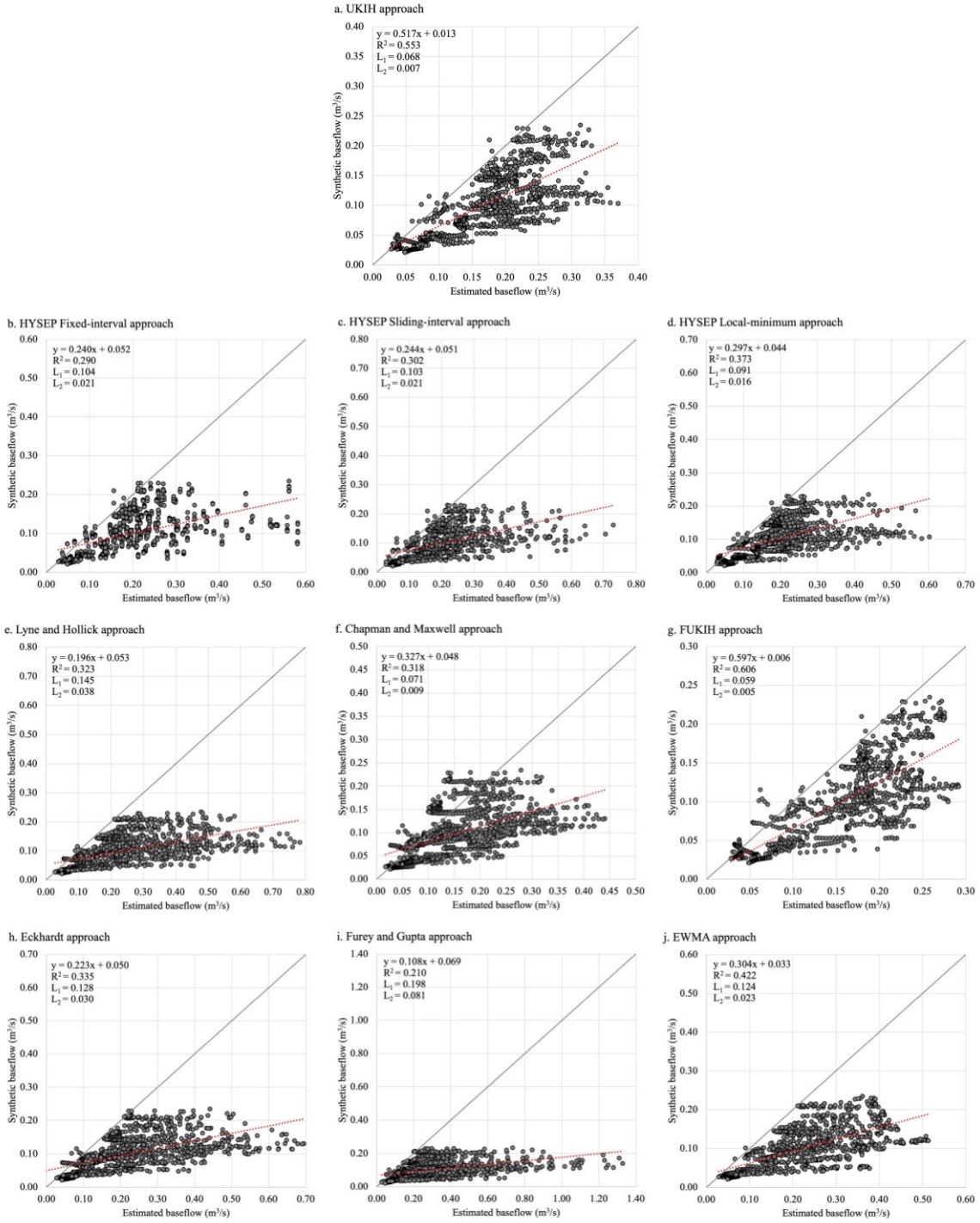

Figure A13. Scatter plots showing the relationship between synthetic baseflow obtained from the HGS model and estimated baseflow at Point 4 calculated through the: a) UKIH; b) HYSEP-Fixed interval; c) HYSEP-Sliding interval; d) HYSEP-Local minimum; e) Lyne and Hollick; f) Chapman and Maxwell; g) FUKIH; h) Eckhardt; i) Furey and Gupta; and j) EWMA approaches. The dashed red lines are the regression lines, while the solid black lines are the 1:1 lines describing a perfect fit.

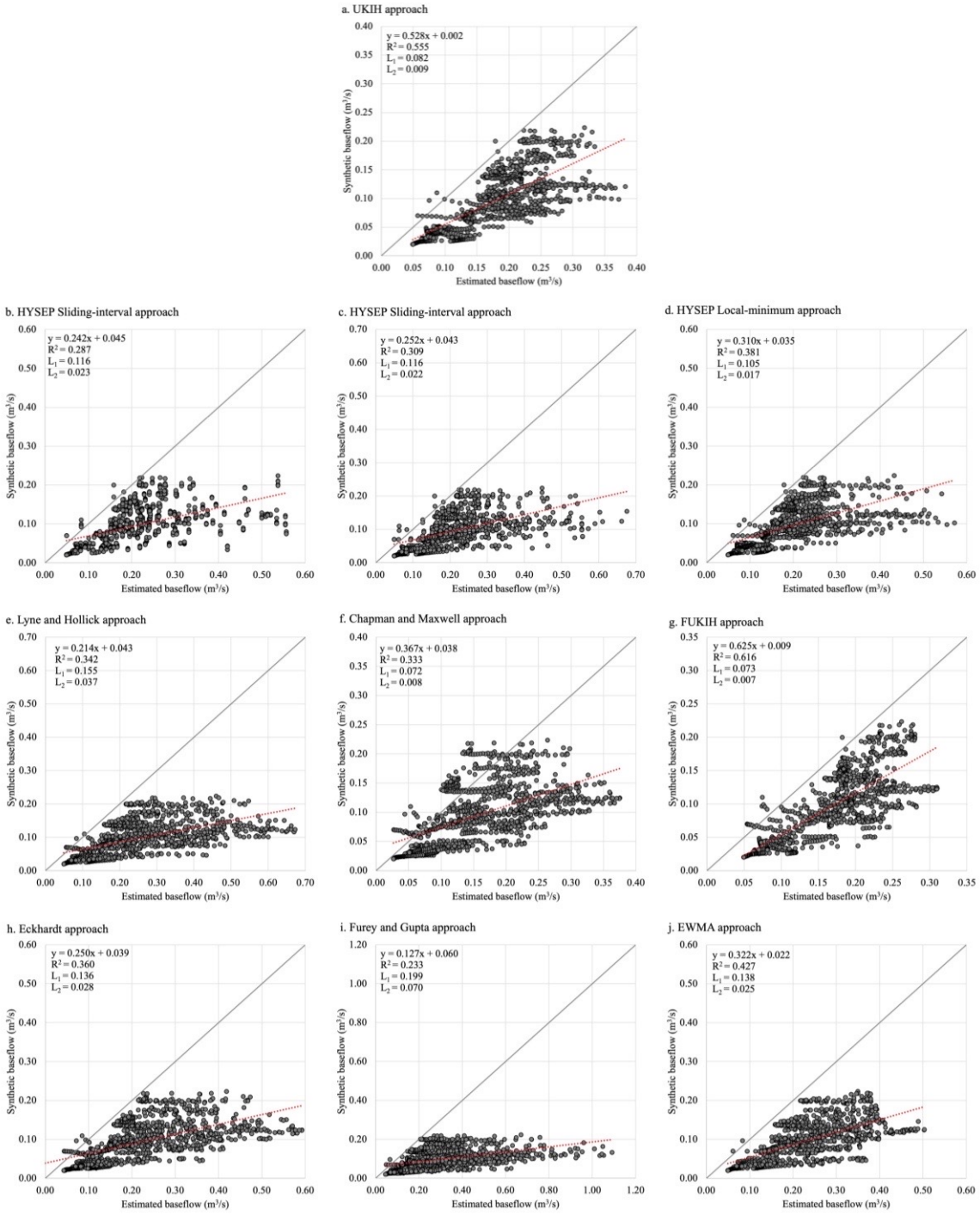

Figure A14. Scatter plots showing the relationship between synthetic baseflow obtained from the HGS model and estimated baseflow at Point 5 calculated through the: a) UKIH; b) HYSEP-Fixed interval; c) HYSEP-Sliding interval; d) HYSEP-Local minimum; e) Lyne and Hollick; f) Chapman and Maxwell; g) FUKIH; h) Eckhardt; i) Furey and Gupta; and j) EWMA approaches. The dashed red lines are the regression lines, while the solid black lines are the 1:1 lines describing a perfect fit.

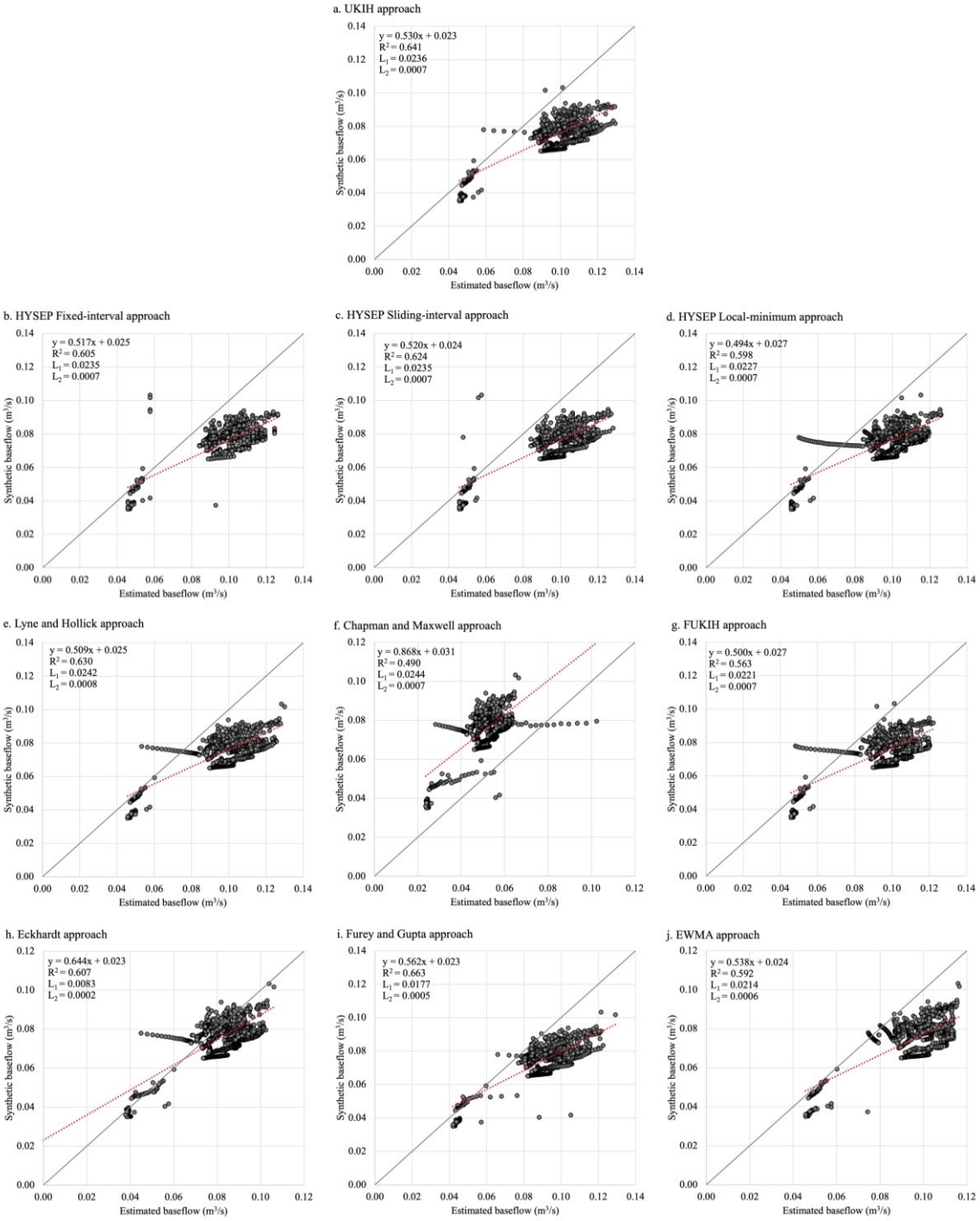

Figure A15. Scatter plots showing the relationship between synthetic baseflow obtained from the HGS model and estimated baseflow at Point 6 calculated through the: a) UKIH; b) HYSEP-Fixed interval; c) HYSEP-Sliding interval; d) HYSEP-Local minimum; e) Lyne and Hollick; f) Chapman and Maxwell; g) FUKIH; h) Eckhardt; i) Furey and Gupta; and j) EWMA approaches. The dashed red lines are the regression lines, while the solid black lines are the 1:1 lines describing a perfect fit.

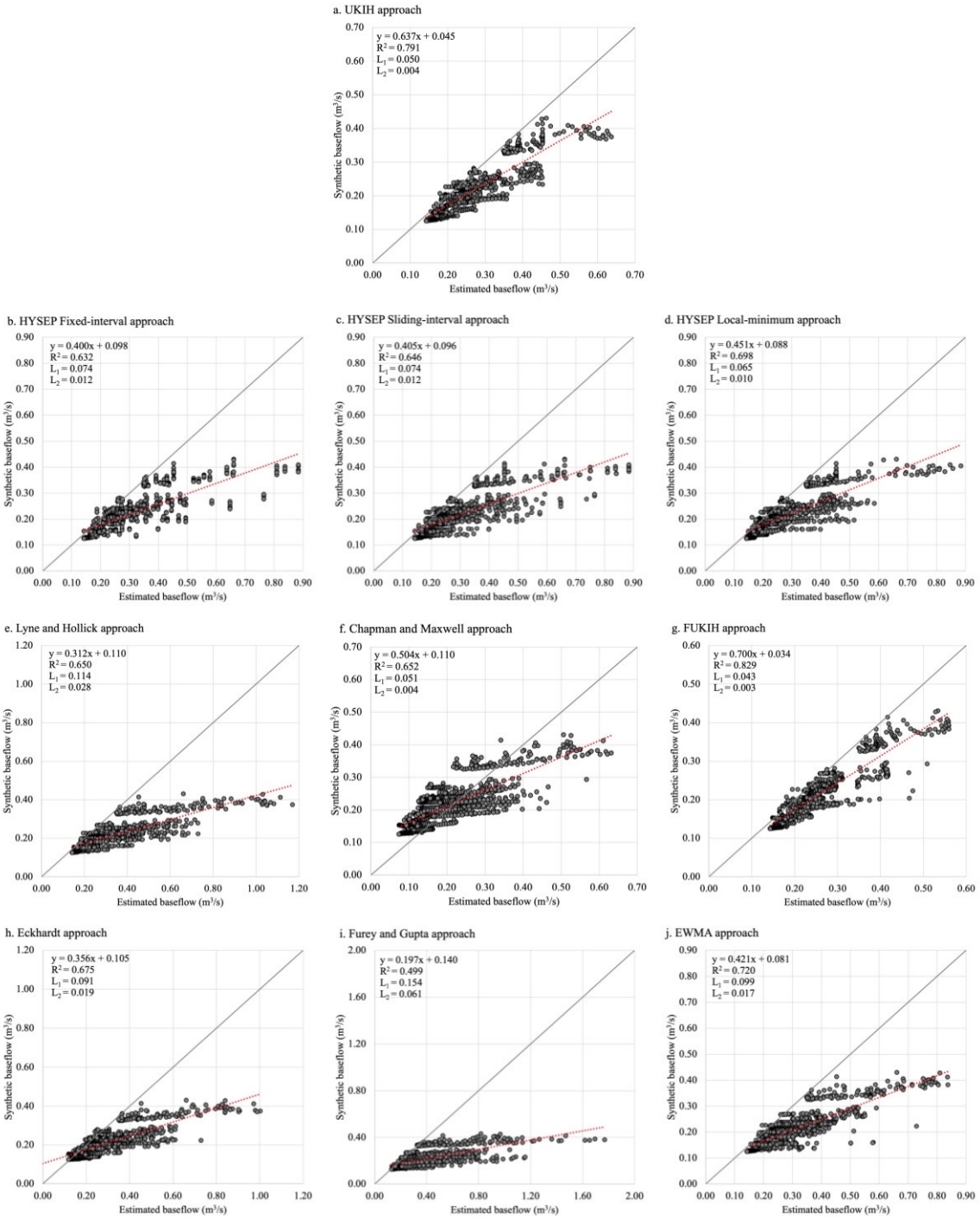

Figure A16. Scatter plots showing the relationship between synthetic baseflow obtained from the HGS model and estimated baseflow at Point 8 calculated through the: a) UKIH; b) HYSEP-Fixed interval; c) HYSEP-Sliding interval; d) HYSEP-Local minimum; e) Lyne and Hollick; f) Chapman and Maxwell; g) FUKIH; h) Eckhardt; i) Furey and Gupta; and j) EWMA approaches. The dashed red lines are the regression lines, while the solid black lines are the 1:1 lines describing a perfect fit.

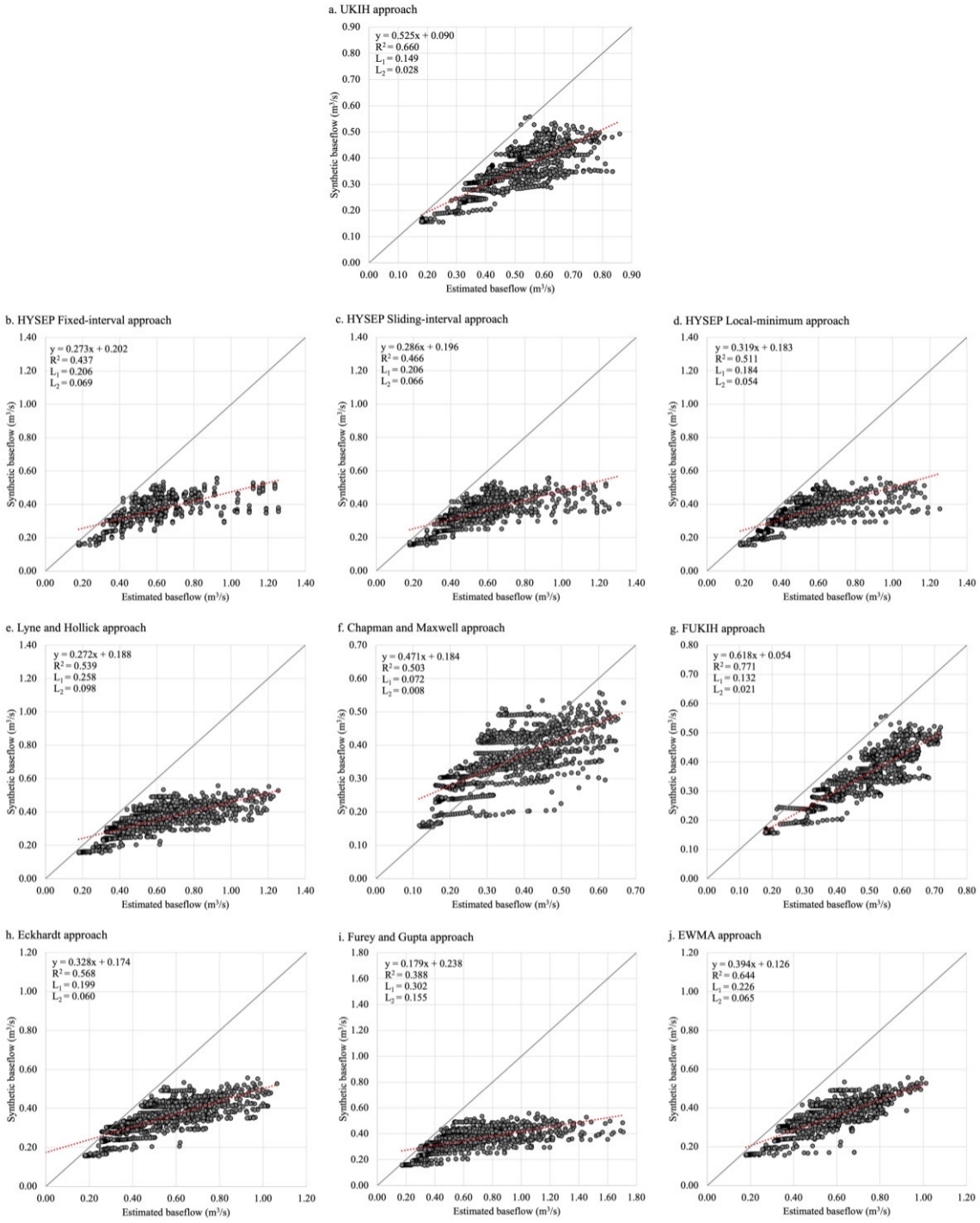

Figure A17. Scatter plots showing the relationship between synthetic baseflow obtained from the HGS model and estimated baseflow at Point 9 calculated through the: a) UKIH; b) HYSEP-Fixed interval; c) HYSEP-Sliding interval; d) HYSEP-Local minimum; e) Lyne and Hollick; f) Chapman and Maxwell; g) FUKIH; h) Eckhardt; i) Furey and Gupta; and j) EWMA approaches. The dashed red lines are the regression lines, while the solid black lines are the 1:1 lines describing a perfect fit.

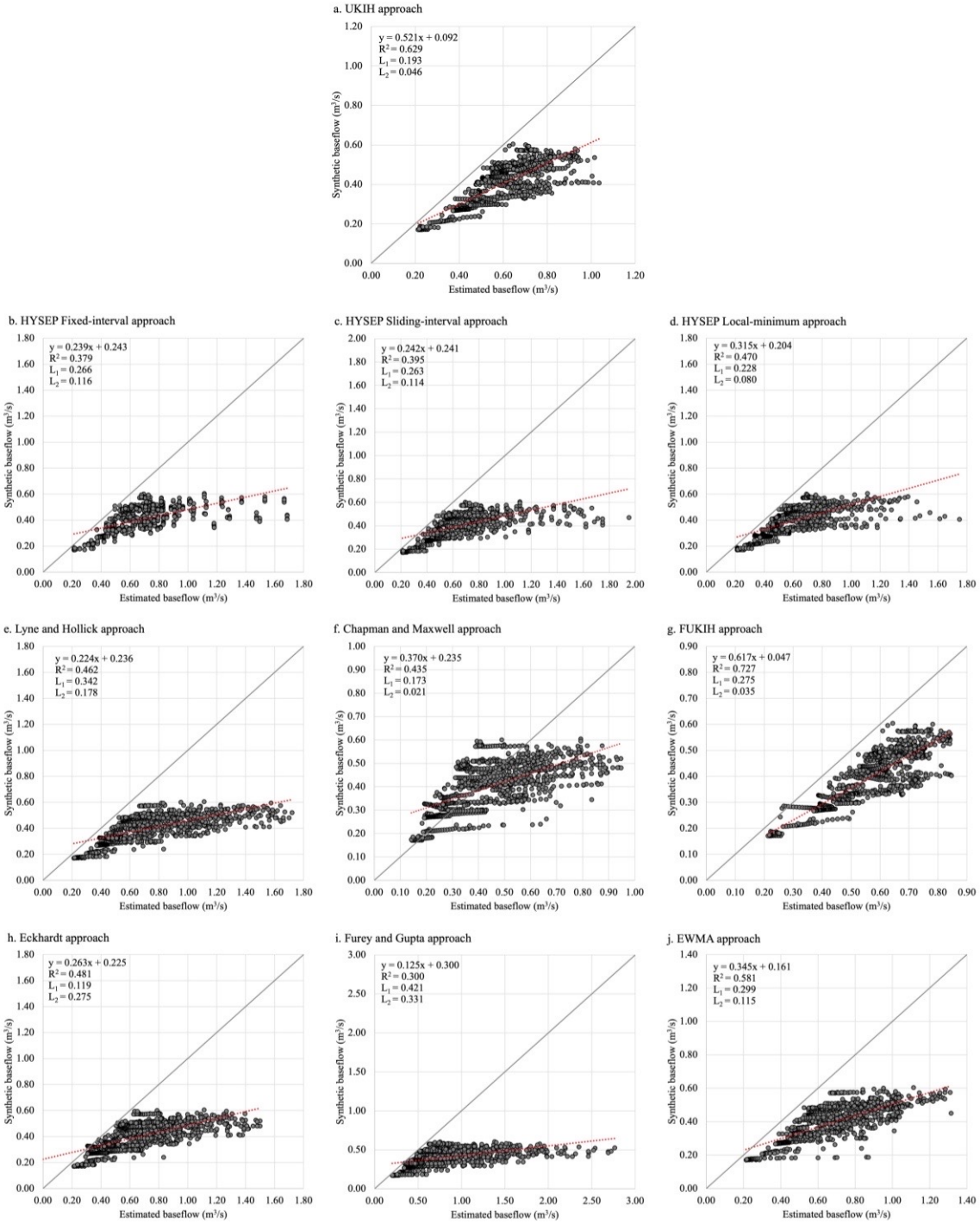

Figure A18. Scatter plots showing the relationship between synthetic baseflow obtained from the HGS model and estimated baseflow at Point 10 calculated through the: a) UKIH; b) HYSEP-Fixed interval; c) HYSEP-Sliding interval; d) HYSEP-Local minimum; e) Lyne and Hollick; f) Chapman and Maxwell; g) FUKIH; h) Eckhardt; i) Furey and Gupta; and j) EWMA approaches. The dashed red lines are the regression lines, while the solid black lines are the 1:1 lines describing a perfect fit.